Economic Geology, v. 105, pp. 119–153

Multistage Intrusion, Brecciation, and Veining at El Teniente, Chile: Evolution of a Nested Porphyry System

V. H. Vry,[1,2] J. J. Wilkinson,[1,2,†] J. Seguel,[3] and J. Millán[3]

[1]*Department of Earth Science and Engineering, Imperial College London, Exhibition Road, London SW7 2AZ, United Kingdom*

[2]*ARC Centre of Excellence in Ore Deposits, Private Bag 126, University of Tasmania, Hobart, TAS 7001, Australia*

[3]*CODELCO División El Teniente, Rancagua, Chile*

Abstract

The El Teniente copper-molybdenum deposit is hosted by the late Miocene Teniente Mafic Complex, a largely subvolcanic package of primarily basaltic-andesite porphyry sills and stocks that were emplaced within the mid-late Miocene Farellones Formation. In the late Miocene-Pliocene, a series of intermediate felsic plutons were intruded into the Teniente Mafic Complex. These are spatially associated with magmatic-hydrothermal breccias and multiple vein types that form individual mineralized complexes.

Here we present detailed observations on mineralogy, textures, and intrusion, breccias, and vein crosscutting relationships to constrain the nature and relative timing of magmatic and hydrothermal events. Our revised classification defines 13 vein types, divided into three main stages: (1) premineralization biotite and/or K-feldspar ± quartz-anhydrite-albite-magnetite-actinolite-epidote veins that formed prior to emplacement of mineralized intrusions and breccias; (2) main mineralization stage veins that grade from gangue-dominated quartz-anhydrite veins ± potassic alteration halos into sulfide-dominated veins with phyllic alteration halos; and (3) late mineralization veins containing sulfosalts. Five breccia types have been observed in the deposit, typically forming individual, vertically zoned complexes, spatially associated with individual intrusions and overlapping in time: (1) igneous-cemented breccias, (2) K-feldspar–cemented breccias, (3) biotite-cemented breccias, (4) anhydrite-cemented breccias, and (5) tourmaline-cemented breccias. Breccia cements display a similar paragenetic evolution to main mineralization stage veins, indicating a close genetic link between them. A distinction can be made between early premineralization vein types (types 1–2) that represent veins formed, possibly deposit-wide, prior to emplacement of intrusion-breccia complexes, late pre- and main mineralization vein types (types 3–8), which are interpreted to reflect the repeated cycle of fluid release associated with each mineralized intrusive complex, and late mineralization vein types (types 9–10) that represent a single event linked to the emplacement of the Braden Breccia Pipe.

The geologic evidence indicates a close spatial and temporal relationship between emplacement of shallow level, felsic-intermediate pipelike intrusions and the development of igneous and mineralized magmatic-hydrothermal breccias and vein halos. The magmatic-hydrothermal transitions observed in these complexes indicate that the deposit formed from a series of localized pulses of magmatic-hydrothermal activity which followed rather similar evolution paths. Single, deposit-wide models of fluid evolution and mineralization are therefore inappropriate. We conclude that El Teniente represents a nested but otherwise rather typical porphyry Cu-Mo system, unusual only in that the Teniente Mafic Complex provided a particularly efficient physical trap in terms of pervasive fracturing during intrusion of magmatic-hydrothermal breccia complexes and as an effective chemical trap for deposition of sulfides. The overlapping of mineralized envelopes from successive fertile intrusions and the absence of barren, intermineral porphyries resulted in its unusual size and high hypogene grades.

Introduction

El Teniente is located on the western margin of the Andean Cordillera in the central Chilean porphyry copper belt and is one of a number of late Miocene-Pliocene copper deposits in the region that also include Los Pelambres and Rio Blanco-Los Bronces (Fig. 1). It is the world's largest copper deposit in terms of contained metal, hosting a premining resource of over 12 billion metric tons of ore with grades averaging 0.65 percent Cu and 0.019 percent Mo.

The deposit has been the subject of a number of published studies (Lindgren, 1922; Howell and Malloy, 1960; Camus, 1975; Skewes et al., 2002; Maksaev et al., 2004; Cannell et al., 2005, 2007; Skewes and Stern, 2007; Klemm et al., 2007), and a significant body of additional descriptive and classification work has been carried out by mine geologists. The earliest description of the orebody was by Lindgren and Bastin (1922) after a short examination in 1917. They proposed that El Teniente represents an andesitic sill-hosted deposit. Howell and Molloy (1960) concluded that mineralization was hosted in an andesitic extrusive flow complex with ore formation linked to the intrusion of a dacite porphyry (Teniente Dacite Porphyry; Fig. 1), based on surface and mine mapping, drill core logging, reconnaissance traverses, and the first thin section petrography. Camus (1975) presented a focused study on the alteration styles at El Teniente, linking mineralization and alteration to the intrusion of multiple quartz diorites and the Teniente Dacite Porphyry. Despite different interpretations of the origin of the host rocks, most early authors agreed that El Teniente represents a classic example of a porphyry deposit with mineralization and alteration concentrically zoned around felsic plutons. However, in several recent papers, Skewes and coworkers (Stern and Skewes, 2002; Skewes et

† Corresponding author: e-mail, j.j.wilkinson@utas.edu.au

0361-0128/10/3867/119-35

Submitted: November 10, 2009
Accepted: December 28, 2009

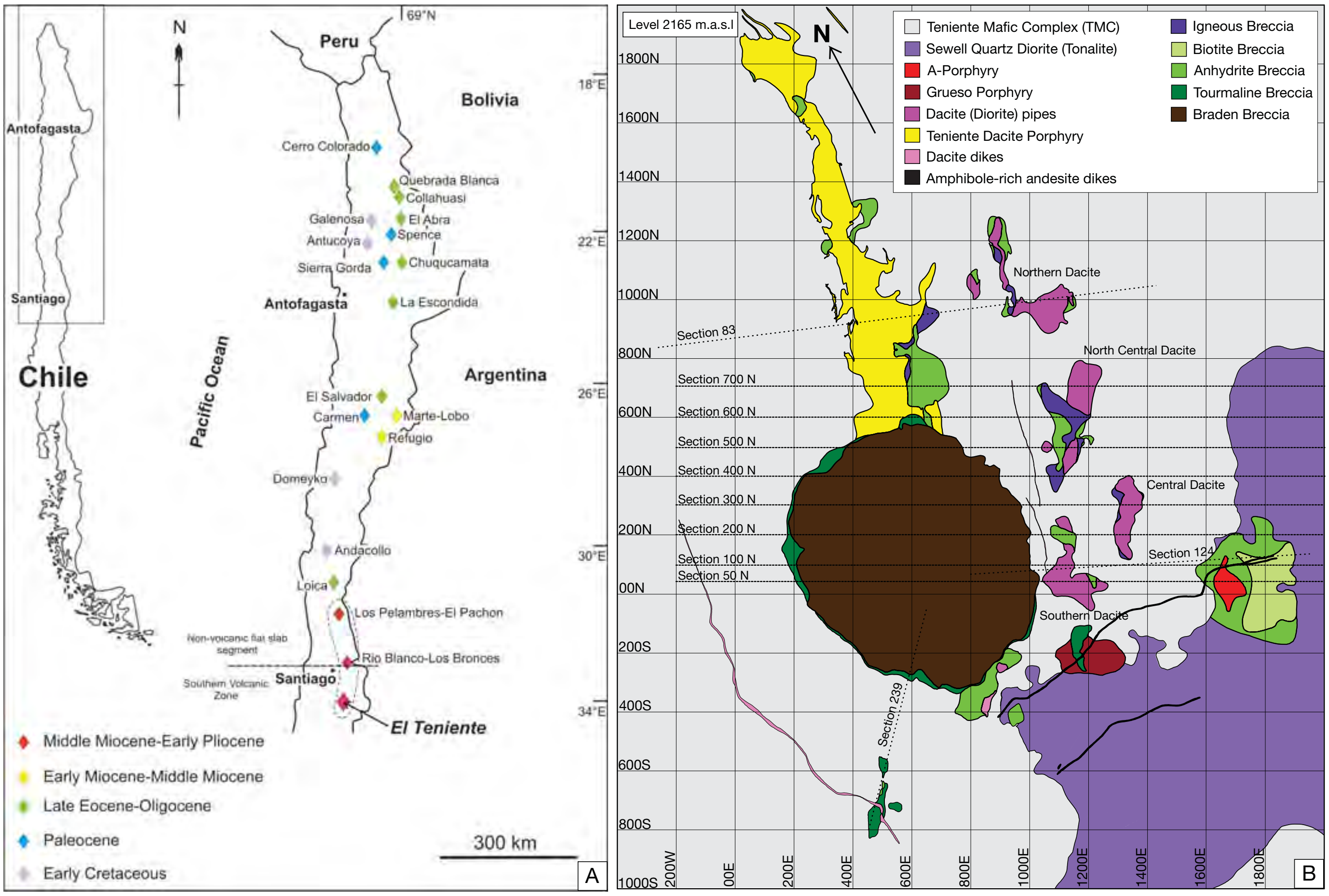

FIG. 1. A. Location map of major porphyry deposits in Chile. El Teniente is situated approximately 100 km south of Santiago in the central Chilean porphyry belt, close to the boundary between two major Andean tectonic segments: the Southern Volcanic zone to the south and the Flat-Slab segment to the north. B. Simplified geologic map of El Teniente level 2,165 m (provided by CODELCO Chile Division El Teniente), showing cross section locations from this study (50N-700N) and others (sections 83, 124, and 239; Skewes et al., 2002; Cannell et al., 2005). Note local mine grid is oriented 14.5°E relative to geographic north.

al., 2005; Skewes and Stern, 2007) redefined El Teniente as a megabreccia deposit with mineralization temporally linked to the emplacement of multiple igneous and hydrothermal breccias prior to, and independently of, the intrusion of felsic plutons (Fig. 2). In contrast, recent geochronology, petrology, vein chronology, structural, and fluid chemistry data (Maksaev et al., 2004; Cannell et al., 2005, 2007; Klemm et al., 2007) were interpreted in terms of more conventional porphyry Cu deposit models (Fig. 2). Equivocal age dates (Maksaev et al., 2004; Cannell et al., 2007; Skewes and Stern, 2007) have hindered the establishment of critical temporal relationships that could distinguish between these alternatives (Fig. 3).

This study presents a review of the geology and classification of host rocks at El Teniente together with detailed field observations of vein, breccias, and intrusion crosscutting relationships. Our purposes are to (1) produce a revised deposit-scale vein chronology; (2) characterize vein types in terms of mineralogy, alteration, and texture; (3) provide robust geologic controls on the relative timing of intrusions, brecciation, and veining; and (4) test and develop existing models for mineralization.

Regional Tectonic and Geologic Setting

El Teniente, along with Río Blanco-Los Bronces and Los Pelambres, is located in the Miocene-Pliocene central Chilean porphyry belt (Fig. 1). These deposits lie close to the boundary between two major Andean tectonic segments: the Southern Volcanic Zone (Stern, 1989; Stern and Skewes, 1995) to the south and the Flat-Slab segment to the north. The Southern Volcanic Zone is characterized by a subduction angle of 30° (Cahill and Isaaks, 1992) and relatively thin crust (35–40 km). In contrast, the Flat-Slab segment is characterized by a subduction angle of 5° to 10° and thicker crust (55–65 km). The steeper angle of subduction in the Southern Volcanic Zone allows for present-day active volcanism, whereas the Flat-Slab segment is inactive.

In the mid-Tertiary, however, the central Chilean magmatic arc sat above a moderately dipping subduction zone. The extensional tectonic regime created a north-south–trending inter-arc volcano-sedimentary basin into which the Oligocene to early Miocene Coya-Machalí Formation (Abanico Formation north of El Teniente; Charrier et al., 2002) was deposited (Camus, 2003). The onset of slab flattening in central

Chile at 15 to 20 Ma, linked to subduction of the Juan Fernández ridge below the South American plate, led to structural inversion, crustal thickening, uplift, and deformation in the Coya-Machalí Formation (Stern and Skewes, 1995; Godoy et al., 1999) with an associated increase in erosion (Skewes and Holmgren, 1993) and eastward migration of the magmatic arc. At approximately 15 to 8 Ma, flat-lying to gently dipping volcanic and volcaniclastic rocks of the Farellones Formation were unconformably deposited on the Coya-Machalí Formation from multiple Miocene volcanic centers.

Several authors have highlighted the importance of tectonic perturbation in the formation of porphyry deposits (Sillitoe, 1997; Kerrich et al., 2000; Cooke et al., 2005; Rosenbaum et al., 2005). The subduction of submarine ridges, oceans plateaus, and seamount chains have been identified as important tectonic "triggers" (Cooke et al., 2005) and, in the case of El Teniente, the subduction of the Juan Fernandez Ridge below the South American plate has been implicated (Stern, 1989; Skewes and Stern, 2005; Skewes et al., 2002; Cooke et al., 2005). It has been suggested that the large volumes of water, sulfur, copper, and chlorine required for porphyry genesis in this area were derived from a mantle source region contaminated by subduction of altered oceanic crust and pelagic and terrigenous sediments (Stern, 1989, 1991; Skewes et al., 2005).

Deposit Geology

El Teniente is hosted by a late Miocene volcano-plutonic complex, referred to as the Teniente Mafic Complex, within the mid-late Miocene Farellones Formation. In the late Miocene-Pliocene, the Teniente Mafic Complex was intruded by a series of felsic-intermediate plutons and multiple igneous and hydrothermal breccia complexes. The central feature of the deposit is a largely postmineralization breccia pipe, which contains the uneconomic Braden Breccia in the core, and an outer shell of mineralized tourmaline breccia. Late mineralization dacite ring dikes and postmineralization amphibole-rich andesite dikes are the youngest intrusive rocks in the El Teniente mine (Fig. 1).

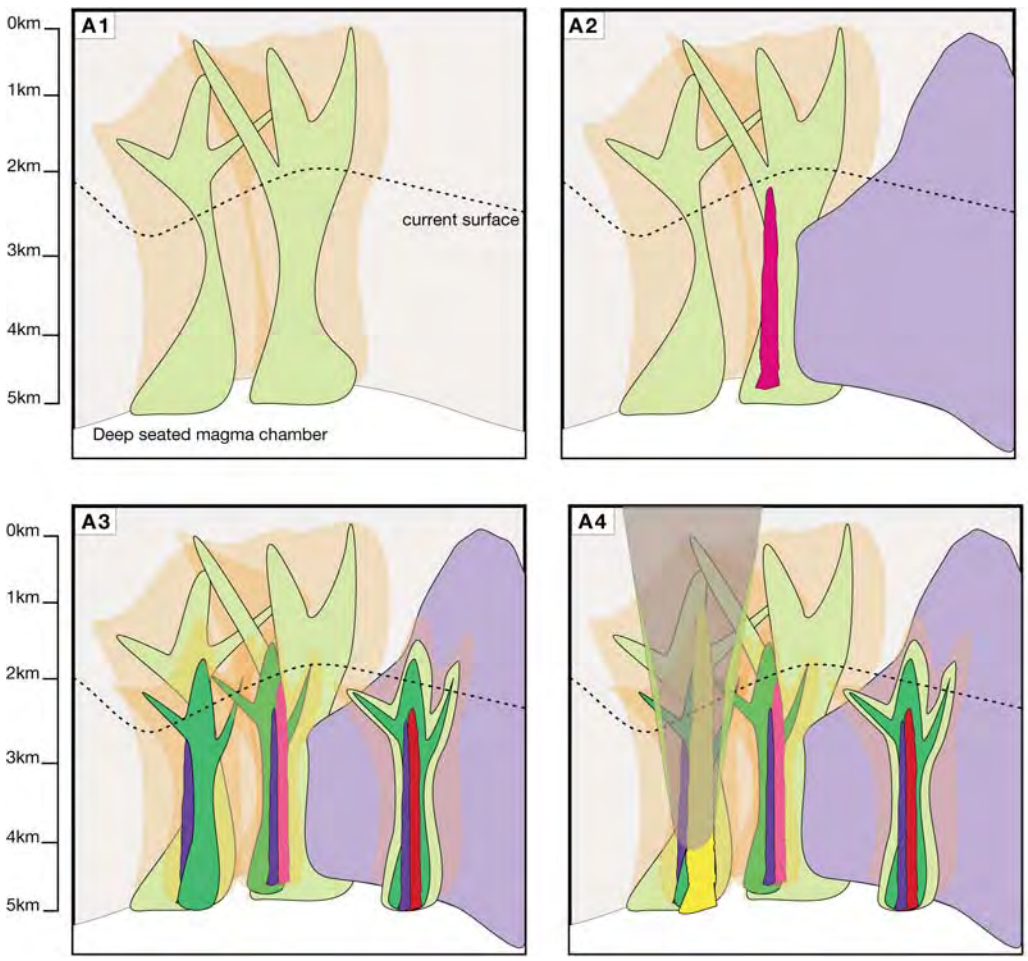

FIG. 2. A. Summary of megabreccia model first proposed by Skewes et al. (2002). (A1). Formation of multiple biotite-cemented hydrothermal breccias derived from fluid exsolution from a deep-seated magma chamber. Formation of these breccias caused widespread deposition of early, high-grade hypogene copper ore with an approximate uniform distribution in the mafic host rocks. (A2). Intrusion of the Sewell Quartz Diorite and dacite finger porphyries in the east of the deposit. (A3). Development of igneous and hydrothermal breccias (biotite-, anhydrite-, and tourmaline-cemented) associated with further localized copper sulfide deposition. (A4). Intrusion of the postmineralization Teniente Dacite Porphyry, which cuts and redistributes earlier mineralization, followed by the formation of the Braden Breccia Pipe.

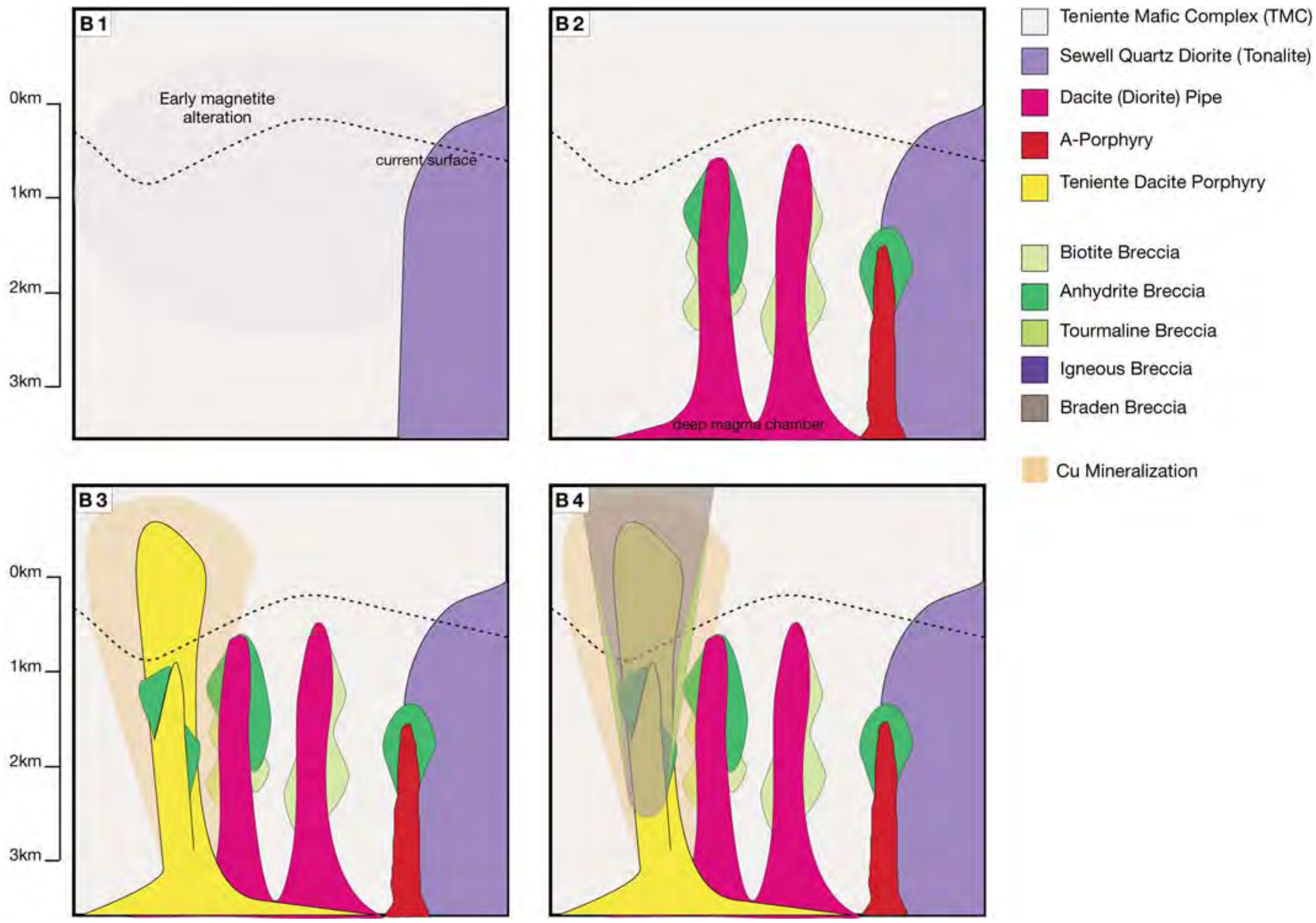

FIG. 2. *(Cont.)* B. Summary of the typical porphyry model (Howell and Malloy, 1960; Camus, 1975; Maksaev et al., 2004; Cannell et al., 2005). (B1). Intrusion of the premineralization Sewell Quartz Diorite, widespread magnetite alteration, and early, premineralization veining in the Teniente Mafic Complex. (B2). Intrusion of the A-Porphyry, and dacite finger porphyries sourced from a deep magma chamber, together with associated magmatic-hydrothermal breccias (biotite-, anhydrite-, and tourmaline-cemented) and main mineralization stage veins. The formation of igneous cemented breccias associated with felsic intrusions are not described in this model. (B3). Multiphase intrusion of the Teniente Dacite Porphyry sourced from an evolved deep magma chamber, accompanied by magmatic-hydrothermal breccias and main mineralization stage veins, followed by late hydrothermal stage veins. (B4). Formation of the Braden Breccia Pipe associated with the development of some late hydrothermal stage veins.

Teniente Mafic Complex

The Teniente Mafic Complex, also referred to as andesites of the mine (Lindgren and Bastin, 1922; Howell and Malloy, 1960), the El Teniente Mafic Intrusive Complex (Skewes et al., 2002), and the Teniente Host Sequence (Cannell, 2004; Cannell et al., 2005), comprises dark green and/or black rocks with aphanitic, porphyritic, and coarser, equigranular textures (Fig. 4A-B; Howell and Molloy, 1960; Skewes et al., 2002; Cannell, 2004; Cannell et al., 2005). In porphyritic rocks the main phenocrysts are labradorite-bytonite plagioclase feldspar (Table 1) that may show flow alignment (Lindgren and Bastin, 1922; Howell and Malloy, 1960; Cannell, 2004), with lesser hornblende and augite. Through most of the mine area these rocks have been flooded with fine-grained biotite (Howell and Molloy, 1960; Skewes et al., 2002; Cannell, 2004). Distally, propylitic alteration has resulted in replacement of hornblende and augite by chlorite and plagioclase phenocrysts by epidote. Above the Teniente-8 mine level strong sericitic alteration is observed.

Cannell et al. (2005) subdivided the Teniente Mafic Complex into nine lithotypes comprising an andesitic sill and stock complex intruded into andesitic lava flows and volcaniclastic units. The predominant intrusive facies was interpreted as andesite porphyry with lesser diorite porphyry, andesite dikes, and minor gabbro. Silica contents for the Teniente Mafic Complex were documented in the range 46 to 57 wt % (basalt to basaltic-andesite), but it was suggested that since pervasive alteration has taken place, original major element concentrations are unknown. Skewes et al. (2002) suggested that andesite is an inappropriate classification for these rocks given the reported silica contents and concluded that the sequence predominantly comprises mafic intrusive rocks including gabbros, diabases, and basaltic andesite porphyries.

Immobile element geochemical discrimination diagrams based on existing and new whole-rock geochemical data

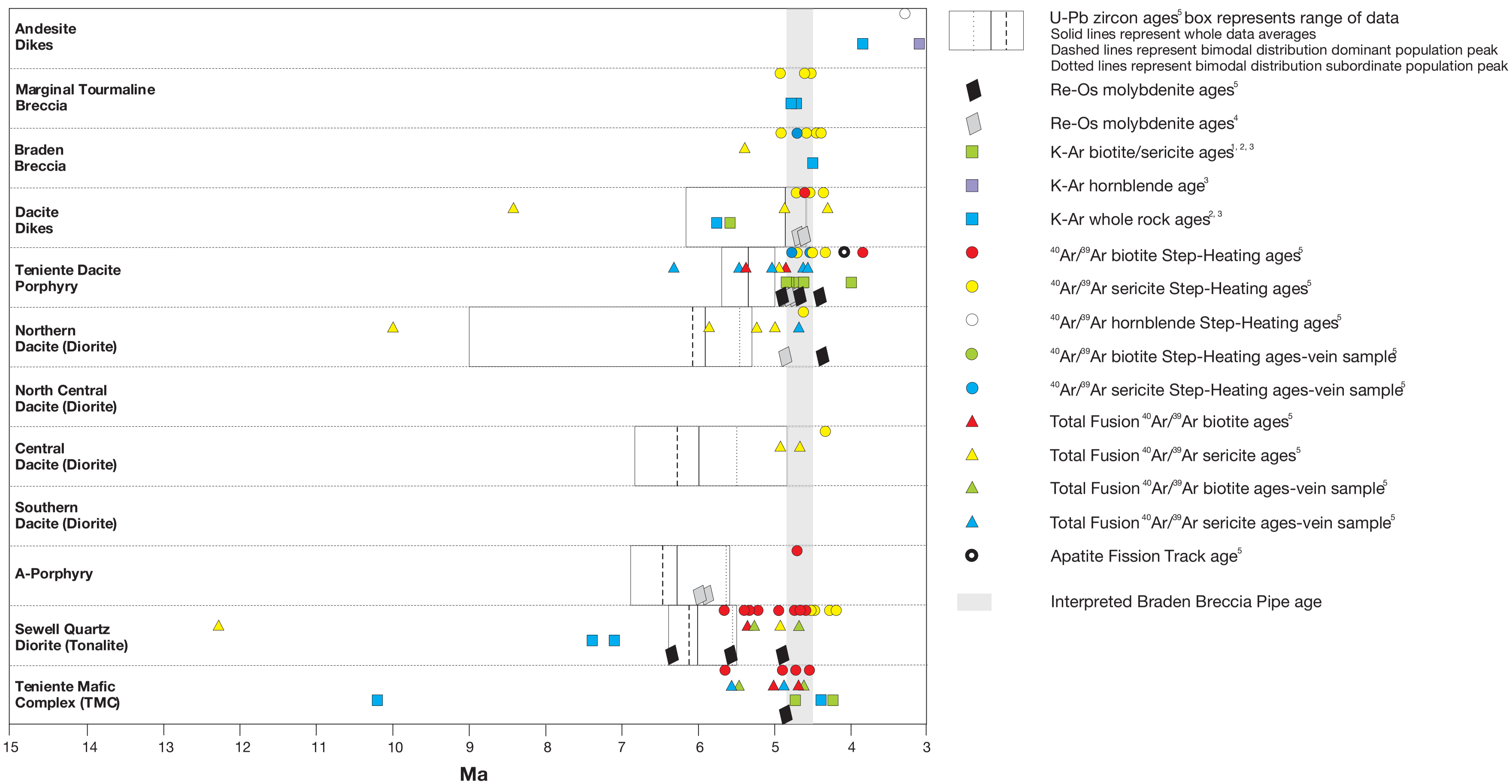

FIG. 3. Compilation of all geochronological data from El Teniente subdivided according to host lithology and possible host-rock age order (oldest at the bottom). [1]Quirt (1972); [2]Clark et al. (1983); [3]Cuadra (1986); [4]Cannell (2004); [5]Maksaev et al. (2004).

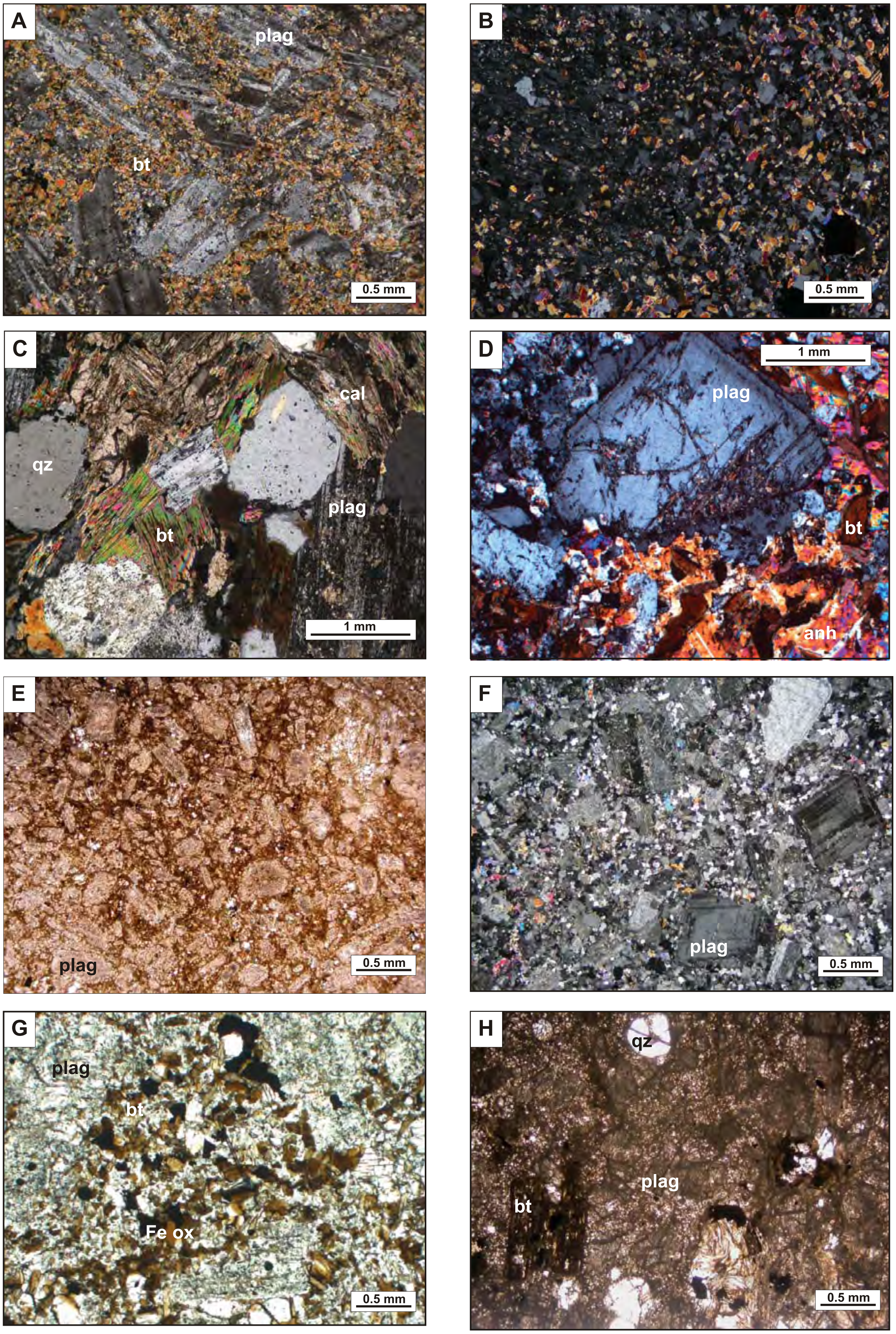
A
plag
bt
0.5 mm
B
0.5 mm
C
cal
qz
plag
bt
1 mm
D
1 mm
plag
bt
anh
E
plag
0.5 mm
F
plag
0.5 mm
G
plag
bt
Fe ox
0.5 mm
H
qz
plag
bt
0.5 mm

TABLE 1. Average Plagioclase Feldspar Analyses from Representative Samples of the Teniente Mafic Complex and Felsic-Intermediate Intrusions

	Teniente Mafic Complex	Sewell Quartz Diorite	A-Porphyry	Grueso Porphyry	North Central Dacite	Teniente Dacite Porphyry	Dacite dike	Andesite dike
Sample no.	08/2512/138	08/2483/12	08/2487/309	07/KC-38/18	08/2240/665	07/2212/141	08/X21/532	07/2333/81
No. of analyses	19	20	12	11	22	14	12	12
Wt %								
Al_2O_3	33.0	24.7	24.4	19.3	21.0	23.1	20.0	30.2
MgO	0.04	0.01	<	0.01	0.20		0.02	1.14
K_2O	0.11	0.29	0.27	1.5	0.73	0.43	0.22	0.69
CaO	16.3	5.9	5.4	0.25	0.41	4.6	0.19	12.0
FeO	0.25	0.25	0.17	0.02	0.21	0.12	0.05	1.1
Na_2O	2.3	8.0	8.3	9.6	10.7	8.3	11.2	3.8
SiO_2	46.5	60.0	60.9	68.0	66.4	60.2	67.4	49.6
TiO_2	0.02	0.01	0.01		0.01			<0.08
Total	98.44	99.04	99.49	98.75	99.70	96.72	99.08	98.62
An%	88.2	44.3	41.4	2.5	3.9	36.9	1.8	75.8
Ab%	11.5	54.4	57.4	88.2	92.0	61.0	96.9	21.6
Or%	0.4	1.3	1.2	9.3	4.1	2.1	1.2	2.6
Average feldspar composition	Bytownite	Andesine	Andesine	Oligoclase	Albite	Oligoclase-Andesine	Albite	Bytownite

Notes: Analysis carried out at the Central Science Laboratory, University of Tasmania; < = below detection

(Table 2, Fig. 5A) suggest that the rocks of the Teniente Mafic Complex were originally mostly basaltic-andesite in composition, with some extending into the andesite field. Because of the predominance of hypabyssal textures (e.g., Cannell et al., 2005), the most abundant rocks of the Teniente Mafic Complex are classified here as basaltic andesite porphyry. Plots of K_2O (and total alkalis; not shown) versus silica indicate a probable original medium K calc-alkaline signature with variable gain in K due to the observed potassic (biotite) ± sericitic alteration. Comparison of measured silica contents with those that can be inferred from immobile element data suggests some silica loss occurred during alteration (cf. Camus, 1975), which can be attributed to replacement of amphiboles and pyroxenes by biotite.

Felsic to intermediate intrusive rocks

The Sewell Tonalite, also referred to as quartz diorite (Lindgren and Bastin, 1922; Howell and Molloy, 1960), located in the southeast of the deposit (Fig. 1), is the oldest felsic-intermediate intrusion at El Teniente (Maksaev et al., 2004) and is generally accepted to have been emplaced premineralization (Lindgren and Bastin, 1922; Howell and Molloy, 1960; Maksaev et al., 2004; Cannell et al., 2005). It consists of an inner phaneritic, equigranular portion composed of andesine-oligoclase plagioclase feldspar (Table 1), altered amphiboles, biotite (Table 3), quartz and minor K-feldspar (Fig. 4C), and an outer phaneritic, porphyritic zone, containing phenocrysts of plagioclase feldspar, biotite and relic amphiboles in a matrix of quartz, plagioclase feldspar, and primary K-feldspar (Skewes et al., 2002). At present it is unclear how the textural variation in this intrusion developed. Camus (1975) attributed this variation to differential cooling with the porphyritic portion representing a chilled margin; Guzmán (1991) suggested that the porphyritic zone represents a separate intrusive phase, perhaps related to the intrusion of the later Teniente Dacite Porphyry. The intrusion exhibits pervasive sericite alteration in its upper levels and minor biotite alteration at greater depths. In deep drill holes it shows intense but patchy magnetite-actinolite sodic-calcic alteration that, in this study, was not observed within any other felsic-intermediate intrusions in the deposit.

Whole-rock geochemical data (Table 2) indicate an intermediate (dioritic) to acidic composition that falls on the same medium K calc-alkaline differentiation trend as the Teniente Mafic Complex (Fig. 5B). There is less geochemical variation and limited K enrichment consistent with the lower degrees

FIG. 4. Photomicrographs of main rock types at El Teniente. (A). Teniente Mafic Complex sample (07/2512/119, DDH2512, 24.00 m) with abundant plagioclase feldspar and pervasive biotite alteration, XPL. It is difficult to distinguish between coarser grained and crowded porphyritic protoliths due to the nature of the biotite replacement. (B). Fine-grained andesite with relatively weak biotite alteration (07/2212/140, DDH2212, 250.20 m), XPL. (C). Equigranular Sewell Quartz Diorite (08/2483/12, DDH2483, 290.80 m) with minor secondary biotite, XPL. (D). Secondary anhydrite(-biotite) in the A-Porphyry replacing a plagioclase feldspar phenocryst or xenocryst (08/2487/309, DDH2487, 391.50 m), XPL. (E). Central Dacite Porphyry (07/2512/132, DDH2512, 110.00 m), PPL. (F). Teniente Dacite Porphyry with plagioclase feldspar phenocrysts and fine silicification and K-feldspar alteration in the groundmass, (07/2212/141, DDH2212, 255.60 m), XPL. (G). Amphibole-rich andesite dike (07/2333/81, DDH2333, 165.40 m), PPL. (H). Grueso Porphyry with plagioclase, biotite, and quartz-eye phenocrysts (07/KC-38/18, Esmeralda Sector), PPL. Abbreviations: anh = anhydrite, bt = biotite, cal = calcite, Fe ox = iron oxide, plag = plagioclase, PPL = plane-polarized light, qz = quartz, XPL = cross-polarized light.

Table 2. Whole-Rock Geochemistry for the Teniente Mafic Complex and Multiple Felsic Intrusions at El Teniente
(data obtained by solution ICP-MS analysis)

	Teniente Mafic Complex				Sewell Quartz Diorite		A-Porphyry			Central Dacite	North Central Dacite	
	DDH1034	DDH1090	DDH2200	DDH2459	08/2483/12	400N	DDH2487	DDH2487	DDH2487	DDH1824	DDH2240	DDH2195
	1044 ft	2817 ft	65 m	681 ft	290.80 m	1780E	391.50 m	401 m	155.10 m	596 ft	444.50 m	20.60 m
Wt %												
Al_2O_3	20.5	18.4	18.3	20.3	17.7	17.8	15.1	14.3	20.4	16.6	16.6	16.1
CaO	8.8	5.4	9.7	7.5	4.4	4.6	13.9	9.3	7.8	2.1	2.4	2.9
Fe_2O_3 (t)	4.9	6.0	5.4	5.5	2.8	3.9	2.9	3.9	8.3	1.8	1.3	1.0
K_2O	2.3	2.6	2.9	2.9	2.5	1.7	4.8	6.4	2.5	5.5	8.1	2.9
MgO	4.2	5.4	4.5	4.4	1.7	1.6	1.4	1.9	5.4	1.2	1.0	1.0
MnO	0.11	0.11	<	<	<	0.10	<	<	0.11	<	<	<
Na_2O	2.6	3.0	4.1	3.6	5.0	6.3	3.7	3.0	3.2	1.6	3.0	5.5
SiO_2	53.2	55.9	48.9	49.1	64.1	61.7	55.7	58.2	49.6	68.5	64.7	68.3
P_2O_5	0.22	0.22	0.24	0.22	0.20	0.19	0.12	0.36	0.22	0.22	0.22	0.22
TiO_2	1.04	0.93	0.82	1.06	0.56	0.57	0.37	0.48	1.25	0.22	0.33	0.27
LOI	0.87	1.68	1.09	0.45	1.20	1.65	0.69	0.71	1.11	1.32	1.65	1.67
Total	98.6	99.6	95.9	95.0	100.1	100.0	98.7	98.5	100.0	99.1	99.3	99.8
(ppm)												
Cu	12800	700	31800	42600	500	400	9700	12900	340	8150	5500	2900
As	18.0	20.8	<	<	4.4	6.4	5.2	<	44.8	3.2	<	<
Ba	65.9	164	233	181	593	546	552	535	188	747	897	474
Be	1.1	1.3	0.85	0.71	1.5	1.2	0.68	0.63	0.78	1.1	1.0	1.0
Bi												
Cd					<	<	<			<		
Co	22.3	35.6	25.4	26.3	8.8	10.3	6.4	35.9	36.7	3.8	40.2	57.6
Cr	62.1	<	31.1	35.5	11.9	23.6	15.0	<	28.2	14.9	10.3	<
Cs	13.4	12.4	13.8	11.2	5.0	3.1	5.5	10.4	14.0	3.1	4.0	2.9
Ga	20.3	19.3	15.4	19.3	20.9	20.3	15.5	19.6	21.7	16.1	15.3	13.8
Ge												
Hf	<	<	<	<	<	<	<	<	<	0.12	<	<
Li	13.1	14.8	19.7	20.3	22.8	8.3	7.3	9.9	13.5	8.2	8.6	7.5
Mo	8.1	20.0	58.0	90.9	2.3	2.3	2.7	3.0	2.1	136	343	151
Nb	3.4	2.7	1.3	1.2	1.9	2.1	1.1	2.4	2.6	8.7	1.1	1.1
Ni	<	23.8	28.7	21.3	9.6	12.6	9.3	<	26.5	7.8	<	<
Pb	3.3	9.3	6.7	3.4	5.9	10.3	6.4	5.2	3.7	10.4	15.5	3.5
Rb	152	147	163	134	95.8	52.6	123	197	138	159	189	82.5
Sb	0.46	0.74	0.20	0.15	0.27	1.0	0.20	0.29	0.44	0.14	0.20	0.16
Sc	26.3	15.8	18.6	27.2	5.6	5.8	3.4	6.5	26.7	4.0	3.8	3.0
Sn	2.1	1.6	1.5	1.2	1.0	0.85	0.92	1.2	1.6	1.1	1.3	1.1
Sr	715	669	919	731	1060	2300	1260	769	808	383	747	601
Ta	0.61	0.64	0.36	0.32	0.29	0.29	0.50	0.75	0.47	0.14	0.64	0.94
Th	2.2	6.3	1.2	1.4	3.7	1.9	1.1	6.9	1.7	2.9	3.3	2.8
Tl	1.0	0.91	0.83	0.47				0.48	1.0		0.87	0.42
U	2.4	0.92	0.41	0.30	1.1	0.91	0.31	1.1	0.34	2.6	1.0	0.22
V	245	195	192	268	113	113	114	167	253	71.7	86.6	62.6
W					4.2	5.8	6.1			11.9		
Y	13.8	10.7	10.1	13.3	4.6	7.4	13.9	10.8	15.0	3.0	2.4	3.1
Zn	34.5	177	31.8	32.5	43.3	125	44.6	32.8	47.7	27.1	19.9	23.7
Zr	120	123	63.7	69.4	179	100	76.0	88.9	79.9	138	111	117
La	10.5	25.3	9.48	8.65	13.4	13.6	24.1	24.5	8.97	14.3	6.42	6.18
Ce	26.5	47.5	20.3	19.9	24.9	28.6	53.4	54.8	21.3	32.8	12.2	10.6
Pr	3.88	5.58	2.74	2.85	2.97	3.75	6.83	7.60	2.96	3.46	1.45	1.24
Nd	16.2	19.5	11.9	12.5	11.5	15.3	27.8	30.3	12.9	11.5	5.55	4.72
Sm	3.97	3.53	2.84	3.25	1.92	2.71	4.51	5.29	3.20	1.42	1.03	0.98
Eu	1.36	1.06	0.77	1.01	0.47	0.64	0.67	0.80	0.96	0.18	0.42	0.44
Gd	3.65	2.90	2.78	3.32	1.47	2.01	3.46	3.85	3.17	1.08	0.77	0.87
Tb	0.56	0.43	0.42	0.51	0.16	0.22	0.36	0.48	0.52	0.11	0.11	0.13
Dy	2.97	2.19	2.21	2.82	0.70	1.02	1.56	2.10	2.94	0.58	0.49	0.64
Ho	0.58	0.44	0.42	0.56	0.12	0.18	0.27	0.38	0.61	0.11	0.09	0.13
Er	1.50	1.17	1.04	1.47	0.30	0.46	0.65	0.89	1.65	0.32	0.23	0.32
Tm	0.21	0.16	0.13	0.20	0.03	0.06	0.07	0.11	0.23	0.05	0.03	0.04
Yb	1.24	0.92	0.71	1.08	0.23	0.36	0.43	0.60	1.38	0.36	0.19	0.25
Lu	0.18	0.13	0.10	0.15	0.03	0.05	0.05	0.08	0.21	0.05	0.03	0.03

Table 2. (Cont.)

	Teniente Dacite Porphyry			Dacite dike	Andesite dike		Grueso Porphyry	Anhydrite breccia matrix	Biotite breccia matrix
	DDH2193 131.80 m	DDH1954 412 ft	DDH1954 909 ft	Diablo sector drift21	DDH2312 194.20 m	DDH2428 2.60 m	Esmeralda sector	DDH2428 186.60 m	DDH2428 186.60 m
(wt%)									
Al_2O_3	16.4	16.3	16.8	15.9	17.8	16.9	15.8	5	12.6
CaO	3.2	2.9	3.1	3.5	6.4	5.6	2.5	61.6	1.1
Fe_2O_3 (t)	<	<	<	2.2	6.0	5.5	0.93	3.0	11.7
K_2O	3.2	3.6	2.9	4.9	1.7	1.6	2.7	3.3	8.9
MgO	0.79	0.89	0.89	0.69	3.8	4.0	0.62	0.53	19.4
MnO	<	<	<	0.1	0.1	0.1	0.1	<	0.11
Na_2O	1.7	1.7	1.7	1.4	4.2	1.7	6.8	0.40	0.11
SiO_2	72.1	72.1	71.4	67.4	58.3	60.9	67.8	23.1	40.7
P_2O_5	0.11	0.11	0.11	0.10	0.30	0.34	0.10	0.26	<
TiO_2	0.20	0.22	0.28	0.31	0.87	0.83	0.30	0.030	3.26
LOI	1.9	1.3	2.6	3.7	0.61	2.2	1.8	2.1	1.5
Total	99.4	99.1	99.7	100.1	100.1	99.8	99.4	99.8	99.5
(ppm)									
Cu	3700	8000	2900	250	80.0	60.0	6000	1900	2200
As	14.3	3.1	7.9	134	8.0	6.6	46.1	<	<
Ba	576	647	568	662	414	375	387	29.0	118
Be	1.5	1.3	1.5	1.4	1.3	1.2	1.0	0.015	1.5
Bi							197		
Cd	<	<	<	<	<	<	0.1		
Co	1.7	1.9	2.3	5.0	21.6	19.6	1.0	7.8	63.2
Cr	7.5	6.8	5.6	8.9	74.6	64.0	8.3	<	48.3
Cs	6.4	3.4	4.3	7.2	2.5	0.6	3.0	0.2	58.7
Ga	18.0	18.0	19.8	17.5	19.7	21.5	11.3	0.6	47.7
Ge							1.6		
Hf	<	<	0.10	<	<	3.0	0.020	<	<
Li	6.2	6.3	5.1	7.9	20.0	10.6	2.3	0.34	21.5
Mo	26.5	18.7	64.1	1.4	3.8	1.5	115	13.9	9.3
Nb	2.7	4.2	*10.1*	2.0	3.4	5.1	1.1	<	20.7
Ni	4.3	4.2	3.8	2.4	44.0	50.5	2.9	<	98.3
Pb	9.4	13.1	6.0	29.6	12.6	7.6	1.9	1.4	3.7
Rb	95.5	85.8	107	190	34.4	27.6	74.4	6.4	643
Sb	1.4	0.36	0.52	11.7	0.93	0.31	0.77	0.14	0.18
Sc	3.1	3.0	3.0	2.5	10.7	11.6	1.5		36.9
Sn	<	0.56	0.49	0.90	1.1	0.84	0.71	0.25	3.1
Sr	639	733	611	264	2350	889	242	1600	76.4
Ta	0.21	0.16	0.17	0.33	0.72	0.32	0.19	0.06	1.4
Th	2.6	3.5	2.4	2.0	2.3	2.2	2.3		1.3
Tl							0.3		1.5
U	0.45	0.88	0.67	0.57	0.61	0.58	0.33	0.07	0.36
V	64.3	59.7	69.1	50.0	137	150	47.9	2.4	616
W	6.0	11.9	17.1	4.1	<	<	22.2		
Y	2.8	2.5	2.4	2.8	12.2	8.7	2.3	29.4	1.5
Zn	23.4	33.5	28.6	48.7	129	79.3	15.4	4.1	117
Zr	89.0	138	109	105	126	135	97.7	<	<
La	11.0	16.8	10.6	14.4	16.4	16.2	10.1	62.3	4.50
Ce	22.7	35.7	20.7	27.5	36.4	37.0	20.4	148	9.12
Pr	2.65	4.03	2.29	3.26	4.82	4.67	2.35	21.52	1.12
Nd	10.4	15.1	8.57	12.1	19.8	19.6	8.85	89.2	4.27
Sm	1.74	2.11	1.36	1.91	3.78	3.78	1.36	16.7	0.72
Eu	0.34	0.23	0.25	0.36	0.95	0.95	0.35	1.94	0.10
Gd	1.20	1.35	0.96	1.34	3.01	2.91	1.20	12.2	0.52
Tb	0.13	0.13	0.11	0.13	0.36	0.35	0.09	1.48	0.07
Dy	0.63	0.62	0.54	0.50	1.71	1.82	0.41	6.05	0.29
Ho	0.10	0.09	0.08	0.07	0.32	0.31	0.06	1.03	0.05
Er	0.23	0.21	0.20	0.18	0.83	0.83	0.19	2.30	0.12
Tm	0.04	0.03	0.03	0.02	0.11	0.12	0.01	0.25	0.02
Yb	0.18	0.17	0.16	0.12	0.71	0.77	0.11	1.26	0.09
Lu	0.03	0.02	0.02	0.01	0.11	0.10	0.01	0.16	0.01

Notes: Samples analyzed by ICP-MS at the Natural History Museum London; < = below detection, blank entries not analyzed; values in italics appear to be anomalous and are therefore not plotted in Figure 5A; due to high sulfide and/or sulfate contents and partial sulfur loss during open vessel digestion, all data have been recast to a sulfur-free basis with Cu included in the major element oxide sum

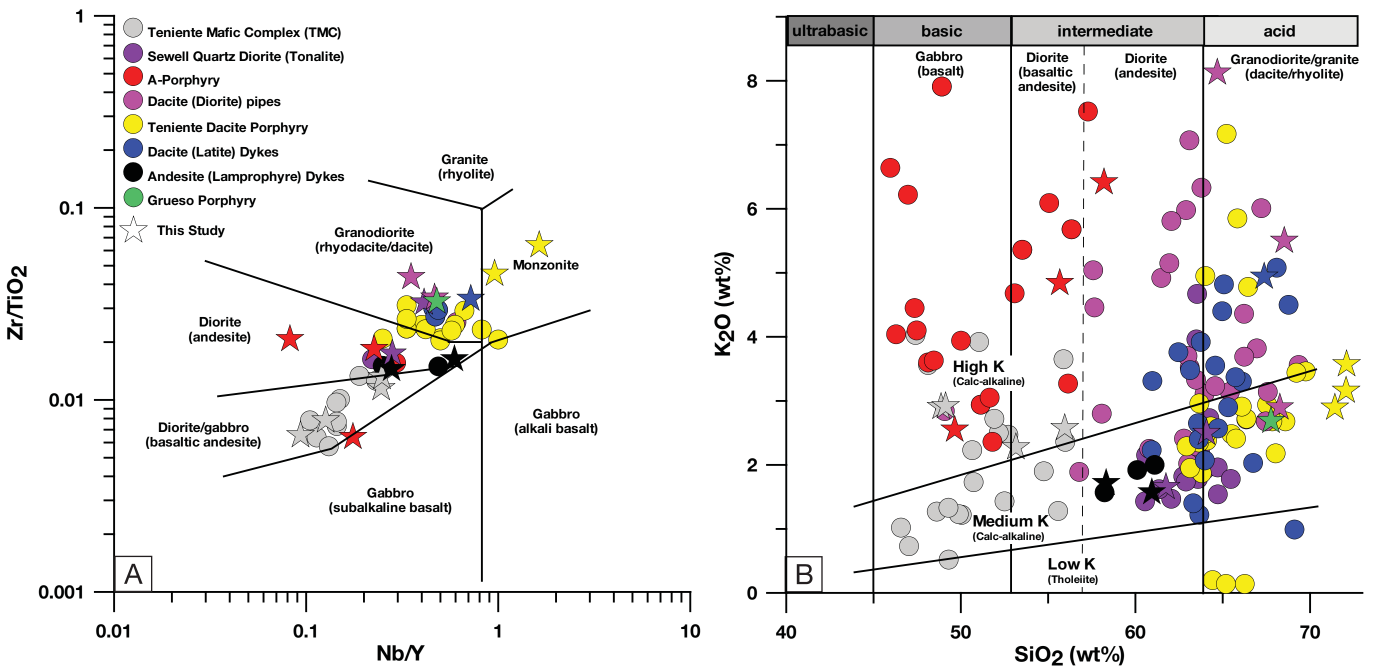

FIG. 5. (A) Trace element (Nb, Y, Zr, Ti) and (B) SiO_2 vs. K_2O discrimination diagrams constructed using whole-rock geochemistry from the Teniente Mafic Complex and the multiple felsic-intermediate intrusions in the deposit. Data from Ossandón (1974), Camus (1975), Riveros (1991), Kay and Kurtz (1995), Skewes (1997, 1998, 2006), Guzmán (2001), Skewes et al. (2002), Rojas (2003), Cannell (2004), Cannell et al. (2005), Funk (2006), and Stern et al. (2007), supplemented with data from this study. Note that the significant dispersion observed in (B) due to potassic alteration is removed in the immobile element plot (A).

of alteration observed, in particular the general lack of potassic alteration. Immobile element geochemistry (Fig. 5A), combined with normative mineralogy calculations that suggest 7 to 15 percent quartz, indicates that the body is better termed the Sewell Quartz Diorite (e.g., Howell and Molloy, 1960).

The A-Porphyry, also referred to as Grey Porphyry (Cannell, 2004; Cannell et al., 2005), was emplaced along the western margin of the Sewell Quartz Diorite at its contact with the Teniente Mafic Complex (Fig. 1). Technically the A-Porphyry is principally a matrix-supported igneous breccia comprising

TABLE 3. Biotite Analyses from Selected Host Rocks, Breccia Cements, Vein Fill, and Vein Alteration Halos

	Sewell Quartz Diorite	Sewell Quartz Diorite	Type 3 alteration	Biotite Breccia matrix	Type 1 vein halo	Type 4a vein halo	Type 5 vein halo
Sample no.	08/2483/12	07/2290/106	07/2459/18	07/2290/104	08/2483/13	07/2290/106	08/2196/771
No. of analyses	8	3	13	17	5	3	5
Wt %							
Na_2O	0.24	0.12	0.22	0.13	0.13	4.30	0.20
SiO_2	37.4	38.9	38.1	39.9	39.1	49.2	37.9
Al_2O_3	15.4	15.4	15.6	13.4	13.7	19.4	18.2
MgO	12.5	16.9	18.4	19.1	18.4	10.0	16.8
K_2O	9.5	9.5	9.6	9.5	8.8	5.5	9.2
CaO	0.04	0.03	0.11	0.01	0.03	0.69	0.04
TiO_2	2.9	3.4	2.9	3.9	1.9	1.0	1.5
Cr_2O_3	0.01	0.02	0.03	0.01	<	0.02	0.01
MnO	0.23	0.18	0.08	0.10	0.13	0.12	0.13
FeO	16.4	10.4	9.5	9.0	12.5	6.2	10.6
NiO	0.03	0.05	0.00	0.00	<	0.01	0.01
ZnO	0.04	<	0.04	0.02	0.02	0.02	0.03
F	0.30	0.64	0.71	0.71	0.43	0.34	0.56
Cl	0.13	0.06	0.07	0.09	0.09	0.05	0.02
Total	95.07	95.60	95.43	95.88	95.24	96.79	95.20

Notes: Analysis carried out at the Central Science Laboratory, University of Tasmania; < = below detection abundant clasts of both the Sewell Quartz Diorite and the Teniente Mafic Complex in a mostly altered matrix of biotite, K-feldspar, andesine-oligoclase plagioclase feldspar, anhydrite, quartz, and sulfides (Cannell, 2004; this study). Clast-free portions have been reported (Stern et al., 2007) but were not observed in this study, either in the available drill holes that intersect the intrusion or during underground mapping of undercut level 2210 or transport level 2165. It has been concluded that the A-Porphyry contains primary magmatic anhydrite (Funk, 2006; Stern et al., 2007) but only secondary (hydrothermal) anhydrite was observed in the present study (Fig. 4D) and by other workers (Cannell, 2004).

Immobile element data suggest that the matrix of the A-porphyry breccia is andesitic in composition (Fig. 5A) and is, with the Sewell Quartz Diorite, the most primitive of the intermediate felsic intrusions in the El Teniente system. Comparison with the mobile element data (Fig. 5B) shows that the rocks are markedly enriched in K_2O, confirming the intense potassic alteration of the igneous matrix noted above. Such potassic alteration is typically associated with high-grade mineralization in the A-porphyry complex and elsewhere in the deposit. Many silica values are well below what would be expected for andesite (as low as 46 wt % in previously published data), implying silica loss during alteration that may in part be related to replacement by anhydrite and/or sulfides (Fig. 4D).

East of the Braden Breccia pipe and northwest of the Sewell Quartz Diorite are four relatively small, finger porphyries (Fig. 1). These are referred to as diorites in current mine terminology, but they have also been referred to as dacite pipes (Cannell et al., 2005, 2007), tonalite pipes (Klemm et al., 2007) and quartz diorite-tonalite stocks (Maksaev et al., 2004. They have a porphyritic texture and consist of 30 to 50 percent plagioclase feldspar phenocrysts (Table 1) plus minor biotite and amphibole phenocrysts, rare quartz eyes, and an aplitic groundmass composed of quartz, plagioclase feldspar, and K-feldspar (Fig. 4E; Cannell, 2004). Previously, plagioclase compositions were reported as albite-oligoclase but those analyzed in the present study from the North-Central Dacite Porphyry (Fig. 1) were predominantly albitic (Table 1). Phenocrysts have been altered to chlorite, sericite, carbonate, and quartz (Cannell, 2004). Immobile element data suggest that these intrusions are dacitic in composition (Fig. 5A) and, in line with the terminology adopted elsewhere in this study, are referred to as dacite porphyries. Potassium shows variable enrichment similar to the A-Porphyry (Fig. 5B), again reflecting the potassic alteration observed in thin section that is associated with high-grade mineralization.

The Teniente Dacite Porphyry, also referred to as a dacite porphyry dike (Cannell et al., 2005), occurs as an approximately 200-m-wide, north-south–trending body extending 1.5 km north of the Braden Breccia Pipe (Fig. 1), beyond the limit of mineralization. It is composed of phenocrysts of oligoclase-andesine plagioclase feldspar (Table 1), biotite, amphiboles, and occasional quartz eyes in a groundmass of quartz, albite, K-feldspar, and biotite (Fig. 4F; Skewes et al., 2002; Maksaev et al., 2004). Many internal mine studies have been carried out on the Teniente Dacite Porphyry (Ossandón, 1974; Duarte, 2000; Rojas, 2003; González, 2006; Hitschfeld, 2006) and multiple intrusive phases are believed to exist based on textural variations and truncated veins. These include: the "euhedral phase," occurring in the northernmost parts of the deposit and along the eastern edge of the intrusive body; and the "subhedral phase," forming the bulk of the southern part of the intrusion. The euhedral phase contains euhedral plagioclase phenocrysts in a fine-grained, typically aplitic matrix. In contrast, the subhedral phase contains plagioclase phenocrysts with resorbed crystal edges and a coarser grained groundmass (Duarte, 2000; Cannell et al., 2005). Rojas (2003) demonstrated that the euhedral phase is younger, containing xenoliths of the subhedral phase. Potassic alteration is observed in the form of secondary K-feldspar in the groundmass (this can be extensive as shown by cobaltinitrite staining); biotite alteration is generally absent. Immobile element data (Fig. 5A) support a dacite classification and the locally intense K-feldspar alteration and silicification (Fig. 4F) are reflected in some elevated K_2O and SiO_2 contents (Fig. 5B). Pervasive sericitic alteration was observed in the upper mine levels along the intrusive contacts (Skewes et al., 2002).

Ring dikes were intruded concentric to the Braden Breccia Pipe and also occur as smaller, northeast-trending dikes (Fig. 1). They have a porphyritic texture comprising mostly albite (Table 1), biotite, and altered amphibole in an aplitic groundmass of quartz and feldspar (Skewes et al., 2002; Cannell et al., 2005). Biotite alteration is absent. Albite phenocrysts are commonly altered to sericite. Whole-rock immobile element data indicate dacitic compositions similar to the dacite porphyries (Fig. 5A). Some samples are enriched in K_2O (Fig. 5B), probably reflecting the observed sericitization.

Postmineralization dikes, referred to both as lamprophyres (Skewes et al., 2002) and amphibole-rich andesites (Maksaev et al., 2004), are the youngest intrusions at El Teniente. They have not been affected by hydrothermal alteration and represent a postmineralization return to more mafic magmatism. They occur as thin, northeast-trending dikes that cut all other intrusions (Fig. 1) and contain amphibole and bytownite plagioclase crystals (Table 1) in a fine-grained groundmass of plagioclase, amphibole, iron oxides, and glass (Fig. 4G; Skewes et al., 2002). Their silica content (Table 2, Fig. 5B) and presence of plagioclase phenocrysts suggest that andesite is the most appropriate classification.

The Grueso Porphyry has not been described previously from El Teniente and occurs along the margin of the Sewell Quartz Diorite and the Teniente Mafic Complex in the south of the deposit (Fig. 1). This stock has a porphyritic texture comprising albite-oligoclase plagioclase feldspar (Table 1), biotite phenocrysts, and quartz eyes in an aplitic groundmass of feldspar-quartz (Fig. 4H). In thin section the Grueso Porphyry appears relatively fresh compared to other felsic rocks in the deposit, although it is still mineralized (e.g., Table 2). Apart from a more sodic character, it shows similar mineralogical and geochemical signatures to the dacite finger porphyries and dacite porphyry dikes (Fig. 5), suggesting a comparable origin.

Breccias

Multiple mineralized igneous and hydrothermal breccias are present at El Teniente. Spatially, these breccias are almost all associated with felsic intrusions (Fig. 1). Five principal breccia types have been previously identified in the mine area (Skewes et al., 2002; Cannell 2004; Seguel et al., 2006): (1) igneous breccias, (2) biotite breccias, (3) anhydrite breccias, (4) tourmaline breccias, and (5) rock flour breccia. Other localized and relatively minor breccia types observed within the deposit and at the district scale include gypsum breccias, magnetite breccias, and actinolite breccias (Skewes et al., 2002; Seguel et al., 2006).

Igneous breccias: These breccias are polymictic, with an altered igneous matrix composed of biotite-quartz-feldspars-anhydrite-chalcopyrite-iron oxides with a holocrystalline, equigranular texture (Skewes et al., 2002). Copper grades are commonly high. They comprise the A-Porphyry stock and occur at the margins of the Teniente Dacite Porphyry and several of the dacite finger porphyries, (Skewes et al., 2002; Cannell et al., 2007; this study).

Biotite breccias: Skewes et al. (2002, 2005) have described widespread biotite-cemented breccias throughout the Teniente Mafic Complex and have suggested that their significance has been obscured due to a lack of visual contrast between them and the biotite-altered host rocks of the Teniente Mafic Complex and overprinting by later brecciation, intrusion, and hydrothermal events. However, no evidence for pervasive brecciation of this type was observed in the present study. Locally, biotite-cemented breccias are well-developed, such as associated with the A-Porphyry (Seguel et al., 2006; Fig. 1) and at the margins of the Teniente Dacite Porphyry and several of the smaller dacite porphyry stocks (Cannell et al., 2007).

Anhydrite breccias: These breccias are polymictic and cemented by hydrothermal anhydrite with minor biotite-tourmaline-quartz-gypsum-apatite-chalcopyrite-pyrite-bornite-rutile (Skewes et al., 2002; Cannell, 2004). They are associated with veins of anhydrite-biotite-quartz-feldspars-sulfides and are typically well-mineralized (Skewes et al., 2002; Cannell et al., 2007). They occur at the margins of the A-Porphyry, the Teniente Dacite Porphyry, and several of the dacite finger porphyries (Fig. 1) and are interpreted to have formed after biotite and igneous breccias (Cannell, 2004; Cannell et al., 2007; this study). Cannell et al. (2007) suggested a syn-Teniente Dacite Porphyry timing for anhydrite breccias adjacent to this intrusion based on crosscutting relationships.

Tourmaline breccias: Dominated by tourmaline, these breccias also contain varying proportions of anhydrite-quartz-chalcopyrite-bornite-pyrite, can be mono- or polymictic, and are mineralized or barren (Skewes et al., 2002). Clasts within the breccias are typically sericitized. Skewes et al. (2002) identified two distinct types of tourmaline breccia: tourmaline breccias in complexes together with biotite and anhydrite breccias, such as the jigsaw-fit breccias associated with the A-Porphyry and described as a "hood of quartz diorite tourmaline breccia" by Camus (1975); and the Marginal Tourmaline Breccia of the Braden Breccia Pipe (Fig. 1). The Marginal Tourmaline Breccia is a tourmaline-rich, polymictic, clast-supported breccia, rich in sulfates, sulfides, and sulfosalts (Skewes et al., 2002). Recently, additional tourmaline breccia bodies have been logged and mapped by mine geologists to the south of the Braden Breccia Pipe (Fig. 1) and small (<100 m), isolated, and sparsely mineralized tourmaline breccia pipes were described as occurring "around the orebody" by Camus (1975).

The Braden Breccia Pipe: The Braden Formation forms the infill of the Braden Breccia Pipe. It comprises two principal facies: a central, subeconomic breccia—the Braden Breccia—and the mineralized Marginal Tourmaline Breccia. The Braden Breccia is a well-consolidated, poorly sorted, polymictic breccia, containing clasts from the surrounding rocks (andesitic porphyry, dacite, and dacite porphyry dikes) as well as extraneous fragments (Howell and Molloy, 1960; Maksaev et al., 2004) set in a rock flour matrix. The Braden Breccia Pipe developed late in the history of El Teniente and appears to have terminated mineralization in the deposit.

Veins

Several studies have been carried out in an attempt to classify vein types at El Teniente (Estándares y Metodologías de Trabajo para Geología de Minas, Capítulo 2, p. 1–25, Superintendencia de Geología, Codelco Chile, División El Teniente, 2003; Valenzuela, 2003; Cannell et al., 2005). The 2003 official mine geology vein classification is based on mineralogy and crosscutting relationships from extensive underground and drill core observations. Fifteen vein types were described, within the three alteration stages defined by Cuadra (1986): the late magmatic stage; the principal hydrothermal stage; and the late hydrothermal stage. Cannell et al. (2005) produced a vein paragenesis divided into four stages, based upon vein mineralogy and crosscutting relationships observed in over 20 km of drill core and thin sections from three cross sections in the deposit, with a focus in and around the Teniente Dacite Porphyry (Fig. 1). In this study we have revised these vein classifications based on new observations from throughout the deposit, including deep drilling not previously available.

Methods

Field data were collected by examination of approximately 7,000 m of core from 30 carefully selected drill holes. These were chosen from eight cross sections across the deposit and from a range of depths, with a focus on intersections of host rock-breccia-intrusion contacts (Fig. 6). These observations were augmented with underground examination of key localities. Crosscutting relationships between the multiple vein types, breccias, and intrusions were described, photographed, and sampled. Over 250 polished thin sections were prepared and studied using transmitted and reflected light petrography; selected samples were examined with scanning electron microscopy to aid in mineral identification and resolve fine-scale textural relationships. This study is built upon field observations carried out during late 2007 through 2008, combined with data from the current mine database on geology, ore mineral, alteration, and grade distribution, and represents the most up to date information available at the time of writing.

Vein Chronology

Thirteen vein types are described within three main paragenetic stages redefined here from earlier work by Cuadra (1986) and Cannell et al. (2005). Within each stage multiple vein types exist (Table 4).

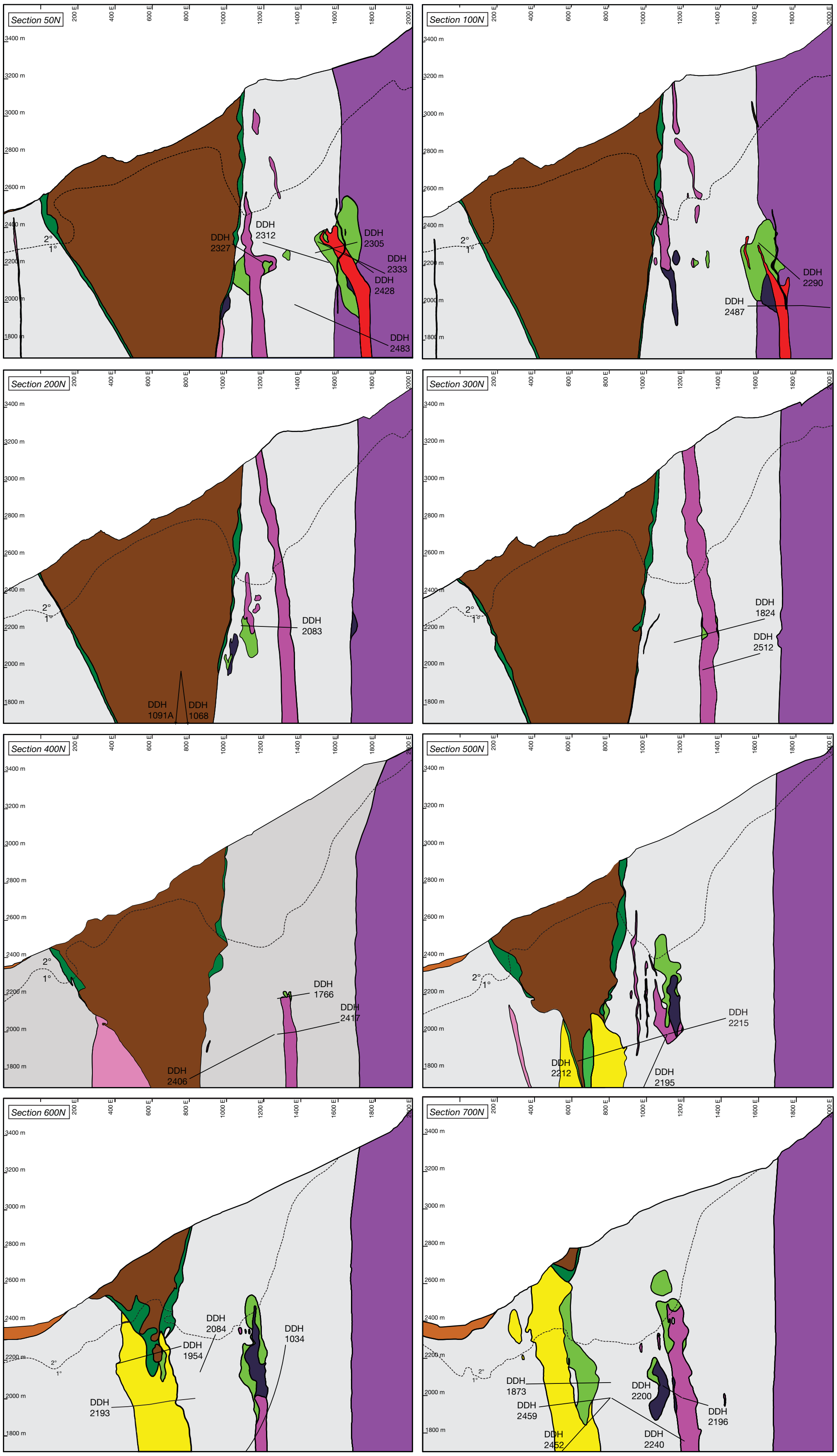

FIG. 6. Geologic cross sections (courtesy of CODELCO Chile División El Teniente), showing the location of drill holes logged in this study. Note: all cores from this study were located within the hypogene ore zone (below dashed line). Lithologic key as for Figure 1. Drill cores DDH1068 and DDH1091A (section 200N) extend an additional 700 m to depth.

TABLE 4. Summary of Vein Paragenesis, Alteration, and Breccia Associations at El Teniente

Vein stage	Vein type	Subtype	Vein mineralogy	Vein halo	Features		Occurrence
Pre-mineralization	1		Biotite-actinolite ± (chlorite-chalcopyrite)	Biotite	Fairly planar, diffuse margin veins		Rare occurrence, associated with deep level magnetite-actinolite alteration in the Sewell Quartz Diorite
	2		Magnetite ± quartz-anhydrite-(chalcopyrite-pyrite)	Unknown original halo			Occur predominantly at deeper levels in the deposit
	3		Biotite-quartz ± anhydrite-(chlorite-chalcopyrite-pyrite-molybdenite)	Quartz-plagioclase	Wavy margin, zoned veins; 5 mm to 3 cm thick		Very abundant throughout the deposit, dominantly in the Teniente Mafic Complex, but also occur rarely in the Teniente Dacite Porphyry
	4	a	Quartz-K-feldspar ± anhydrite-apatite-biotite	Biotite	Diffuse-planar veins; 1 to 5 mm thick		Very abundant throughout the deposit, dominantly in the Teniente Mafic Complex, but also occur in the Sewell Quartz Diorite and the A-Porphyry
		b	K-feldspar-epidote-anhydrite-chlorite ± quartz	Local epidote	Planar veins; 1 to 5 mm thick		Rare occurrence close to the Teniente Dacite Porphyry at depth and on deposit periphery; distal equivalents of type 4a
Main Mineralization	5		Anhydrite-quartz ± chalcopyrite-pyrite-bornite-molybdenite	Biotite halo in mafic hosts, K-feldspar/no halo in felsic hosts	Irregular to planar veins; 5 mm to 4 cm thick		Occur throughout the deposit
	6	a	Quartz-anhydrite-K-feldspar ± chalcopyrite-molybdenite-bornite-pyrite	Occasional thin K-feldspar halo in felsic hosts	Straight margin, planar veins; typically 5 mm to 4 cm thick	Veins form a continuum from quartz dominated end members to sulfide dominated end members	Formed synchronously with thick, up to 8 m, quartz dikes; most abundant in and around the Teniente Dacite Porphyry and dacite pipes; bornite most common in veins of this type in and around the Teniente Dacite Porphyry
		b	Quartz-chalcopyrite-anhydrite-K-feldspar ± molybdenite-pyrite-(bornite)	Occasional thin K-feldspar halo in felsic hosts	Straight margin, planar veins; typically 5 mm to 4 cm thick; contain a central sulfide seam, dominantly chalcopyrite with molybdenite selvage; these veins are interpreted type 7a veins overprinted by later stage 8 veins		
	7	a	Molybdenite ± (quartz-anhydrite)	No halo	Thin, up to 5 mm, typically <2 mm, sulfide veins		Molybdenite-rich vein most abundant in the dacite pipes
		b	Chalcopyrite ± (quartz-anhydrite)	No halo			
	8		Chalcopyrite-pyrite-quartz-anhydrite	Sericite-chlorite-quartz	5 mm to 8 cm thick chalcopyrite dominated veins with wide, well-developed, and often zoned sericite-chlorite-quartz halos		Abundant throughout the deposit, in the Teniente Mafic Complex, all felsic intrusions and crosscutting all breccia types
Late Mineralization	9		Tourmaline-carbonate-anhydrite ± chalcopyrite-pyrite-bornite-molybdenite	Sericite-chlorite-quartz	Thick, up to 8 cm, tour dominated veins with wide, well-developed sericite-chlorite-quartz halos	Veins form a continuum from tourmaline bearing to carbonate bearing	Most abundant close to the Braden Breccia Pipe, associated with the development of the Braden Breccia?
	10		Carbonate-anhydrite-gypsum ± tennantite-chalcopyrite-pyrite-bornite-molybdenite	Sericite-chlorite-quartz	Thick, up to 8 cm, veins with wide, well-developed sericite-chlorite-quartz halos		

Premineralization stage veins

The premineralization stage represents early alteration and veining prior to the deposition of significant amounts of Cu-Mo sulfides. Early premineralization stage veins (types 1 and 2; Fig. 7A-B) contain minor Cu-Mo sulfides; however, much of this is attributed to overprinting from later vein stages (e.g., Fig. 7C). The premineralization stage is characterized by pervasive, widespread magnetite alteration which has been extensively overprinted and destroyed by later veining and alteration events and is therefore usually only preserved at deeper levels within the mine or as residual patches within the Teniente Mafic Complex (cf. Skewes et al., 2002; Cannell et al., 2005).

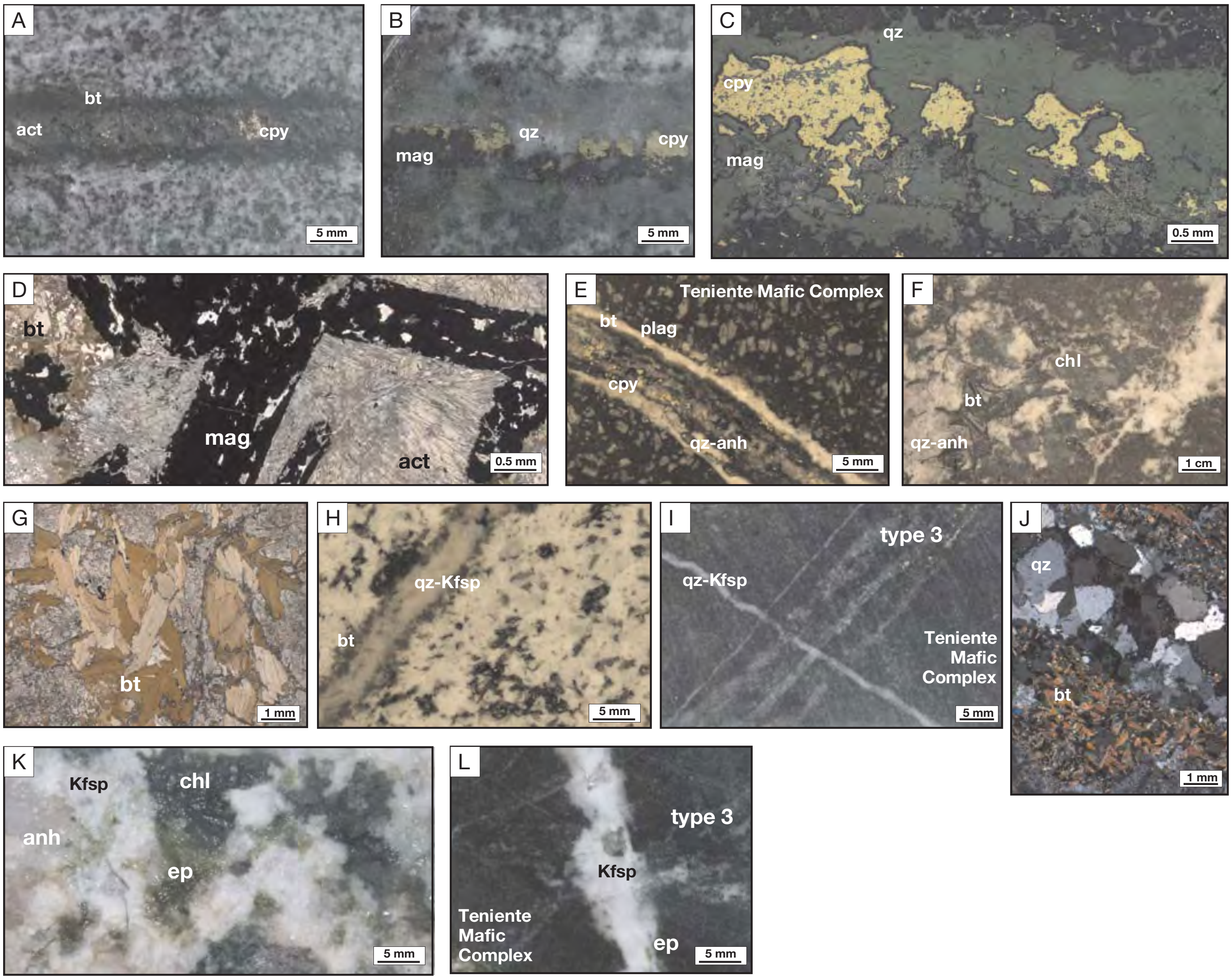

FIG. 7. Premineralization stage vein and alteration types. (A). Biotite-actinolite(-chlorite) type 1 vein with diffuse biotite halo in the Sewell Quartz Diorite (08/2483/13, DDH2483, 294.90 m), hand specimen. Later chalcopyrite overprints the vein and is disseminated in the wall rock. (B). Magnetite-quartz-secondary chalcopyrite type 2 vein in Sewell Quartz Diorite (08/2483/02, DDH2483, 201.40 m), hand specimen. (C). Reflected light photomicrograph of sample shown in (B), illustrating chalcopyrite replacing magnetite, related to a type 8 vein overprint, RL. (D). Actinolite-magnetite alteration, associated with type 1 veins, overprinted by biotite located at depth within the Sewell Quartz Diorite (08/2483/63, DDH2483, 499.00 m), PPL. (E). Complexly banded type 3 vein in the Teniente Mafic Complex (07/2512/138, DDH2512, 127.85 m), hand specimen. (F). Irregular, patchy alteration with type 3 vein mineralogy in the Teniente Mafic Complex (07/2459/23, DDH2459, 89.20 m), hand specimen. (G). Coarse biotite associated with type 3 alteration patches within the Teniente Mafic Complex as shown in (F) (07/2459/17, DDH2459, 61.10 m), PPL. (H). Type 4a K-feldspar-quartz vein with wide, diffuse biotite halo in the Sewell Quartz Diorite (07/2290/106, DDH2290, 173.90 m), hand specimen. (I). Type 4a vein cuts type 3 vein in the Teniente Mafic Complex (08/2195/687, DDH2195, 59.50 m), hand specimen. (J). Thin biotite halo associated with a type 4a vein in the Teniente Mafic Complex (08/2193/434, DDH2193, 403.50 m), XPL. (K). K-feldspar-anhydrite-epidote(-chlorite) type 4b vein (08/1034/71, DDH1034, 3050 ft), hand specimen. (L). Type 4b vein cuts type 3 vein in the Teniente Mafic Complex (08/1034/74, DDH1034, 3055 ft), hand specimen. Abbreviations: act = actinolite, anh = anhydrite, bt = biotite, chl = chlorite, cpy = chalcopyrite, ep = epidote, Kfsp = K-feldspar, mag = magnetite, plag = plagioclase, PPL = plane-polarized light, qz = quartz, RL = reflected light, XPL = cross-polarized light.

Type 1 veins: These veins are characterized by a biotite-actinolite ± (chlorite-chalcopyrite) assemblage (Table 4), with chlorite produced by later alteration of early biotite. Chalcopyrite probably represents a later overprint and has normally replaced biotite. Veins from this stage are typically planar with straight vein walls and diffuse biotite halos. Biotite halos show relatively high FeO (12.5 wt %) contents compared to later vein stages (Table 3). These veins occur at depth in the mine within the Sewell Quartz Diorite, proximal to locally pervasive zones of biotite-actinolite-magnetite-(chlorite) ± K-feldspar alteration (Fig. 7D). Their mineralogy suggests a relationship to the transition between inner propylitic (amphibole-stable) and potassic alteration zones.

Type 2 veins: These veins consist principally of magnetite ± quartz-anhydrite-(chalcopyrite-pyrite; Table 4, Fig. 7B) and have undulating or planar walls. Sulfides in these veins typically overprint magnetite (Fig. 7C) and are interpreted to represent vein infill from later stage veins, most likely sulfide-rich main mineralization stage veins (type 8) based on the co-occurrence of quartz-sericite-chlorite alteration halos that are characteristic of this later vein stage (Fig. 8M-N). No evidence of any original alteration halos has been observed. These veins occur at deeper levels in the mine, both in the Teniente Mafic Complex and the Sewell Quartz Diorite.

Type 3 veins: These veins are abundant in the Teniente Mafic Complex and are composed of zoned biotite-quartz- ± anhydrite(-chlorite-chalcopyrite-pyrite-molybdenite) with wavy-edged, diffuse walls and diffuse quartz-feldspar halos (Table 4, Fig. 7E). Typically they comprise an inner quartz ± anhydrite seam flanked by biotite-chlorite grading into a diffuse quartz-plagioclase (andesine-labradorite) halo (Table 5). Chlorite in these veins appears to be related to secondary alteration of original biotite. The anhydrite component in these veins varies from completely absent to dominant. These veins commonly appear to have been reopened by later sulfide-dominated vein stages, as evidenced by central, sulfide-rich seams in many examples. Diffuse alteration patches that are mineralogically similar to type 3 veins and are inferred to be related to them are common in the Teniente Mafic Complex (Fig. 7F-G).

Type 4a veins: These veins are dominated by K-feldspar (Table 5) with lesser quartz, minor anhydrite, apatite, and biotite and are characterized by thin biotite halos characterized by relatively high Na_2O and low MgO contents compared to other vein halos (Table 3). They predominantly occur in the Teniente Mafic Complex where they form thin (<2 mm) straight-edged veins often occurring as a dense stockwork. They have also been observed in the Sewell Quartz Diorite and A-Porphyry where they tend to be thicker (1–5 mm) with wider, more diffuse biotite halos (Table 4, Fig. 7H). Type 4a veins consistently crosscut type 3 veins (Fig. 7I). Biotite halos on type 4a veins in the Teniente Mafic Complex can be difficult to identify (e.g., Fig. 7I) but are clearly seen in thin section (Fig. 7J).

Type 4b veins: These veins are rare and appear to be spatially restricted to deep levels and on the deposit periphery, mainly close to the Teniente Dacite Porphyry and on the southern margin of the system. They are composed of K-feldspar-epidote-anhydrite-chlorite ± quartz with a local epidote alteration halo (Tables 4, 5; Fig. 7K). They have been observed cutting type 3 veins (e.g., Fig. 7L) and to be cut by later type 6 veins. Their mineralogy suggests a relationship to inner propylitic zone alteration.

Main mineralization stage veins

Previously defined as two stages, the late magmatic stage and the principal hydrothermal stage (Villalobos, 1975; Cuadra, 1986; Cannell et al., 2005), we have combined these to reflect what we regard as an evolution in vein formation during mineralization rather than distinct stages. The main mineralization stage is characterized by thicker, straighter veins, with early types dominated by quartz-anhydrite that may grade

FIG. 8. Main mineralization stage vein and alteration types. (A). Planar type 5 anhydrite vein cutting the North-Central Dacite Porphyry (08/2200/772, DDH2200, 7.90 m), hand specimen. (B). Irregular type 5 anhydrite vein with thin biotite halo in the Teniente Mafic Complex (08/2196/771, DDH2196, 96.00 m), hand specimen. (C). Type 6a quartz-K-feldspar vein in the Teniente Mafic Complex cutting type 3 and 4a veins (07/2459/16, DDH2459, 58.30 m), hand specimen. (D). Type 6a quartz-K-feldspar vein in the Teniente Dacite Porphyry (08/1873/541, DDH1873, 984 ft), hand specimen. (E). SEM-CL image illustrating the granular texture and weak-moderate growth zoning in type 6a veins (07/2212/141, DDH2212, 255.60 m). (F). Chalcopyrite-dominated main mineralization stage type 8 vein with associated sericitic alteration cutting a type 6a quartz vein (07/2459/35, DDH2459, 163.80 m), XPL. (G). Thick type 6b quartz vein with molybdenite-rich outer zones and central chalcopyrite seam, possibly fed from thin veinlets (type 7b) that crosscut the molybdenite-rich quartz (07/2512/119, DDH2512, 24.00 m), hand specimen. (H). Photomicrograph of part of vein shown in (G), showing central sulfide seam and location of SEM-CL images (07/2512/119, DDH2512, 24.00 m), PPL. (I). SEM-CL image of (H), showing quartz textures within the type 6b vein. Multiple generations of quartz are present, with clasts of original vein quartz entrained within later sulfide vein fill (07/2512/119, DDH2512, 24.00 m). (J). SEM-CL image of (H), showing fractures in quartz prior to sulfide, together with late quartz overgrowths likely to be related to subsequent sulfide vein fill (07/2512/119, DDH2512, 24.00 m). (K). Quartz-dominated type 6a vein cuts an earlier anhydrite-dominated type 5 vein in the Teniente Mafic Complex (08/1873/494, DDH1873, 276 ft), hand specimen. (L). Thin type 7a molybdenite vein with silicification halo cut by type 7b chalcopyrite vein in the Central Dacite Porphyry (07/2512/123, DDH2512, 35.10 m), hand specimen. (M). Chalcopyrite-pyrite-quartz type 8 vein with wide sericite halo (07/2290/102, DDH2290, 167.60 m), hand specimen. (N). Thick chalcopyrite-pyrite type 8 vein with wide, banded sericite-chlorite halo in the Teniente Mafic Complex (08/2487/176, DDH2487, 46.90 m), hand specimen. (O). SEM-CL image of a type 8 vein, illustrating euhedral quartz growth and partly planar, partly dissolved (lower-right) boundaries between quartz and sulfides (08/2483/08, DDH2483, 223.50 m). (P). Photomicrograph showing rounded early pyrite grains surrounded and partly replaced by chalcopyrite in a type 8 vein (08/2487/180, DDH2487, 102.00 m), RL. Abbreviations: act = actinolite, anh = anhydrite, bt = biotite, chl = chlorite, cpy = chalcopyrite, ep = epidote, Kfsp = K-feldspar, mag = magnetite, mo = molybdenite, plag = plagioclase, PPL = plane-polarized light, py = pyrite, qz = quartz, RL = reflected light, SEM-CL = scanning electron microscopy cathodoluminescence, ser = sericite, XPL = cross-polarized light.

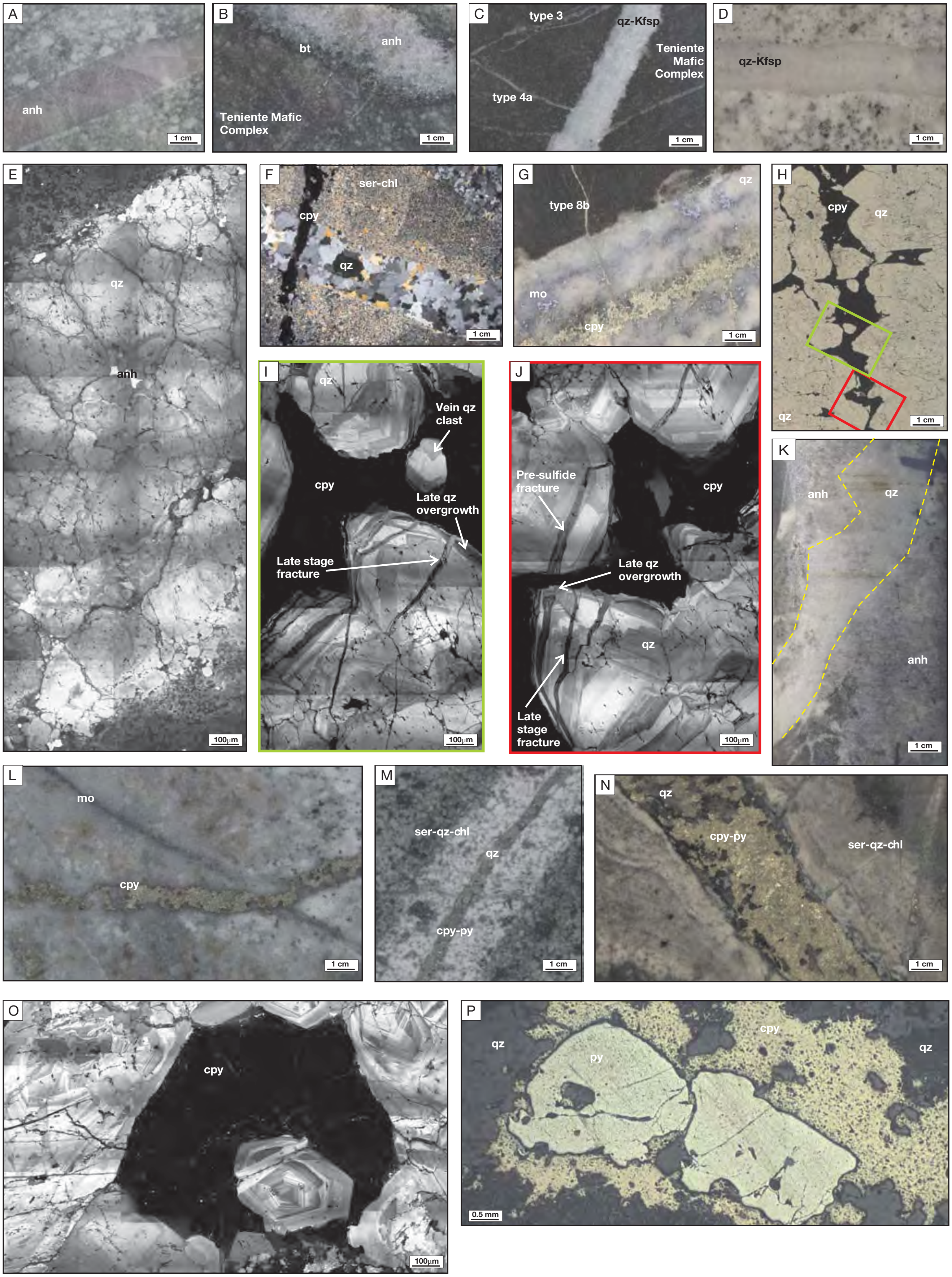
A
anh
1 cm
B
bt
anh
Teniente Mafic Complex
1 cm
C
type 3
qz-Kfsp
Teniente Mafic Complex
type 4a
1 cm
D
qz-Kfsp
1 cm
E
qz
anh
100µm
F
ser-chl
cpy
qz
1 cm
G
type 8b
qz
mo
cpy
1 cm
H
cpy
qz
qz
1 cm
I
qz
Vein qz clast
cpy
Late qz overgrowth
Late stage fracture
100µm
J
Pre-sulfide fracture
cpy
Late qz overgrowth
qz
Late stage fracture
100µm
K
anh
qz
anh
1 cm
L
mo
cpy
1 cm
M
ser-qz-chl
qz
cpy-py
1 cm
N
qz
cpy-py
ser-qz-chl
1 cm
O
cpy
100µm
P
qz
py
cpy
qz
0.5 mm

TABLE 5. Feldspar Analyses from El Teniente Breccia Cements, Vein Fill, and Alteration Halos

	Igneous Breccia cement[2]	K-feldspar breccia (K)[1]	K-feldspar breccia (Na)[1]	Type 3 vein halo[2]	Type 4a vein infill[2]	Type 4b vein infill[2]	Type 6a vein infill[2]	Type 6b vein infill[2]
Sample no.	08/2240/632	07/2290/114	07/2290/115	08/2512/138	07/2290/106	08/1034/71	08/2212/141	08/2193/388
No. of analyses	19	5	3	16	6	11	9	6
Wt %								
Al_2O_3	23.7	17.9	19.4	26.3	18.8	19.2	17.8	18.6
MgO	0.01	<	<	0.07	0.01	0.02	0.01	0.01
K_2O	2.4	15.1	0.37	0.33	15.8	13.4	13.8	16.0
CaO	4.4	<	0.49	7.5	0.01	0.03	0.10	<
FeO	0.10	<	<	0.13	0.05	0.03	0.05	0.01
Na_2O	7.5	1.0	11.0	6.9	0.93	2.4	1.7	0.83
SiO_2	61.8	64.2	66.8	57.5	63.5	64.3	61.5	63.3
BaO		0.62						
TiO_2	0.01	<	<	0.10	<	<	0.01	0.02
Total	99.88	98.41	98.01	98.75	99.12	99.33	94.91	98.76
An%	34.9	0.0	4.6	54.0	0.1	0.3	1.1	0.0
Ab%	53.7	9.4	93.3	44.6	8.2	21.4	15.3	7.3
Or%	11.4	90.6	2.1	1.4	91.7	78.4	83.7	92.6
Average feldspar composition	Oligoclase-andesine	Orthoclase	Albite	Andesine-labradorite	Orthoclase	Orthoclase	Orthoclase	Orthoclase

Notes: Blank entries not analyzed; < = below detection
[1] Analysis carried out at the Natural History Museum London
[2] Central Science Laboratory, University of Tasmania

into the later, sulfide-dominated types. Veins in the early part of this stage typically lack alteration halos (Table 4) except where overprinted by later veins. This is a marked distinction from the premineralization stage veins described above. Late veins within this stage mark the transition to feldspar-destructive alteration with the widespread development of sericite-quartz-chlorite alteration associated with complex, chalcopyrite(±other sulfide)-rich veins (Table 4). This phyllic alteration is dominant in the upper levels of the mine and has a rather sharp base at level Teniente-8 (1,983 m.a.s.l.).

Type 5 veins: These veins are dominated by anhydrite with minor amounts of quartz ± chalcopyrite-pyrite-bornite-molybdenite and have irregular or planar walls (Table 4). They occur throughout the deposit both in felsic intrusive rocks, where they have poorly developed K-feldspar halos or no alteration halos (Fig. 8A), and in the Teniente Mafic Complex, where they have thin biotite halos (Table 3, Fig. 8B).

Type 6 veins: These veins are mineralogically similar to type 5 veins but are dominated by quartz with minor K-feldspar-anhydrite ± chalcopyrite-molybdenite-bornite-pyrite (Tables 4, 5, Fig. 8C-D). They are thick (4 mm–5 cm), planar, straight-edged veins with a granular texture (Fig. 8E-F) and lack alteration halos in the Teniente Mafic Complex except where overprinted by later vein stages (e.g., Fig. 8F). This vein type is abundant in the deposit occurring in the Teniente Mafic Complex and all felsic-intermediate intrusions. Type 6a veins occurring in and around the Teniente Dacite Porphyry typically contain bornite as the dominant sulfide; those occurring within and proximal to the multiple dacite finger porphyries commonly contain abundant molybdenite. Chalcopyrite-bearing type 6a veins occur throughout the deposit. Quartz-dominated type 6a veins are interpreted to be commonly reopened by, or are transitional to, later veins (e.g., types 7 and 8) forming composite type 6b veins with a central, sulfide-rich, quartz-poor seam (Fig. 8G). Evidence for partial dissolution of original vein quartz resulting in truncation of growth zones and replacement by a quartz-chalcopyrite-pyrite assemblage is seen in SEM-cathodoluminescence images (Fig. 8H-J). Type 6b veins are also abundant throughout the deposit. These quartz-dominated veins cut anhydrite-dominated type 5 veins (Fig. 8K). These veins are noticeably more abundant close to the Teniente Dacite Porphyry, and their abundance decreases with depth.

Type 7 veins: These veins reflect a transition from silicate- to sulfide-dominated veins. They occur as two principal types: molybdenite-dominated (7a); and chalcopyrite-dominated (7b). They occur as thin (mostly <1 mm) sulfide ± minor quartz-anhydrite veins lacking alteration halos (Table 4). Chalcopyrite-rich type 7b veins are abundant throughout the deposit. Molybdenite-rich type 8a veins are most abundant in the dacite finger porphyries and are always cut by the more abundant chalcopyrite-rich type 7b veins (Fig. 8L). These sulfide-dominated veins are thought to be the most important within the vein sequence in terms of copper introduction.

Type 8 veins: These veins are often thick (5 mm–4 cm), planar, straight-edged, chalcopyrite-dominated veins with lesser pyrite-quartz-anhydrite (Table 4, Fig. 8M-N), although some veins of this type can be dominated by pyrite. Little molybdenite and no bornite have been observed. In contrast to type 6b veins (Fig. 8I-J), SEM cathodoluminescence reveals euhedral quartz intergrown with chalcopyrite and pyrite with little or no truncation of quartz growth zones (Fig. 8O). Typically, pyrite is early and is partially replaced by later chalcopyrite, leaving relic-rounded grains of pyrite (Fig. 8P). Vein halos tend to be wide (3 mm–3 cm), are well developed in both mafic and felsic hosts, and are typically zoned from an inner quartz-sericite assemblage to an outer chlorite-rich assemblage. Multiple paler and darker green bands are commonly observed in the wider alteration halos. This vein type occurs throughout the deposit; however, its abundance is notably lower in and around the Teniente Dacite Porphyry and at depth.

Late mineralization stage veins

The late mineralization stage is characterized by the precipitation of carbonates and tourmaline in veins and the occurrence of wide sericite-quartz-chlorite vein halos. Their mineralogy can vary greatly between individual examples and even along the length of a single vein. Late mineralization stage veins are most abundant proximal to the Braden Breccia Pipe.

Type 9 veins: These veins are dominated by tourmaline which occurs with an assemblage of carbonate-anhydrite ± chalcopyrite-pyrite-bornite-molybdenite (Table 4). These veins are commonly thick (up to 8 cm) with well-developed, wide sericite-quartz-chlorite halos (Fig. 9A-C). Tourmaline typically lines the edges of the veins, with a central carbonate fill (Fig. 9C-D).

Type 10 veins: These veins are predominantly composed of carbonate-anhydrite-gypsum with lesser chalcopyrite-tennantite-pyrite-bornite-molybdenite (Table 4, Fig. 9E-J), although mineral proportions can vary greatly. In many of these veins gypsum has replaced carbonates and anhydrite (Fig. 9J). The veins tend to be coarse grained and can contain large, isolated crystals and clots of sulfides (Fig. 9J). They are commonly thick (up to 8 cm) with wide sericite-quartz-chlorite halos.

Breccia Facies

Breccia bodies form important hosts to high-grade mineralization at El Teniente. Those examined in the present study are spatially associated with the A-Porphyry, the Central Dacite Porphyry, the North-Central Dacite Porphyry, the Northern Dacite Porphyry, and the Teniente Dacite Porphyry. These are described in terms of their mineralogy, texture, morphology, and spatial occurrence, summarized in Table 6.

Igneous breccias

Igneous breccias are present in spatial association with all of the felsic-intermediate intrusions at El Teniente (Figs. 1, 6, 10A-G). They are mainly located on the sides and/or upper parts of these intrusions, occurring as thin, vertically elongate shells along the contact with the country rocks. All igneous breccias observed in the present study are cemented by a crystalline, porphyritic igneous rock comprising plagioclase feldspar phenocrysts in a matrix overprinted by biotite-quartz and disseminated sulfides (Fig. 10A, G). Plagioclase phenocrysts from an igneous breccia associated with the North-Central Dacite Porphyry have intermediate oligoclase-andesine compositions (Table 5) compared to the dacite itself, which has plagioclase phenocrysts with more sodic compositions, possibly suggesting two different intrusive events (Table 1). They are typically matrix supported and chaotic, with subangular to subrounded polymictic clasts, millimeter to centimeter in size. Clasts are typically locally derived from

TABLE 6. Summary of Breccia Facies Present at El Teniente

Breccia type	Breccia matrix mineralogy	Breccia clast types	Features and occurrence	Crosscutting vein relationships
Igneous	Oligoclase-andesine feldspar phenocrysts, biotite-quartz-sulfides ± anhydrite	Teniente Mafic Complex, Sewell Quartz Diorite, dacite	Occurs at the margins of felsic intrusions, as vertical intrusive bodies	Cut by vein types from 5 onwards
K-feldspar	K-feldspar-albite ± biotite	Teniente Mafic Complex, Sewell Quartz Diorite, dacite	Coarse-grained K-feldspar, found at deep levels in the deposit within the Sewell Quartz Diorite adjacent to the A-Porphyry	Cut by type 8 veins
Biotite	Biotite ± chalcopyrite	Teniente Mafic Complex, Sewell Quartz Diorite, dacite	Coarse grained (up to several cm) biotite matrix; occurs adjacent to the A-Porphyry	Cuts type 4a veins in the Sewell Quartz Diorite and A-Porphyry; cut by type 6b and 8 veins
Anhydrite	Anhydrite ± chalcopyrite ± molybdenite	Teniente Mafic Complex, Igneous breccia, dacite	Coarse-grained anhydrite cement with abundant sulfide deposition; occur adjacent to all felsic-intermediate intrusions in the deposit; gradation between biotite and anhydrite breccias in the A-Porphyry complex	Cuts type 3 and 4 veins close to dacite pipes and Teniente Dacite Porphyry; cut by type 6a veins
Tourmaline	Tourmaline ± anhydrite ± chalcopyrite ± molybdenite	Teniente Mafic Complex, dacite	Historically reported to occur at high level above the A-Porphyry; occurs above the Grueso Porphyry, south of the Braden Breccia Pipe and as the outer marginal component of the Braden Breccia Pipe	None observed

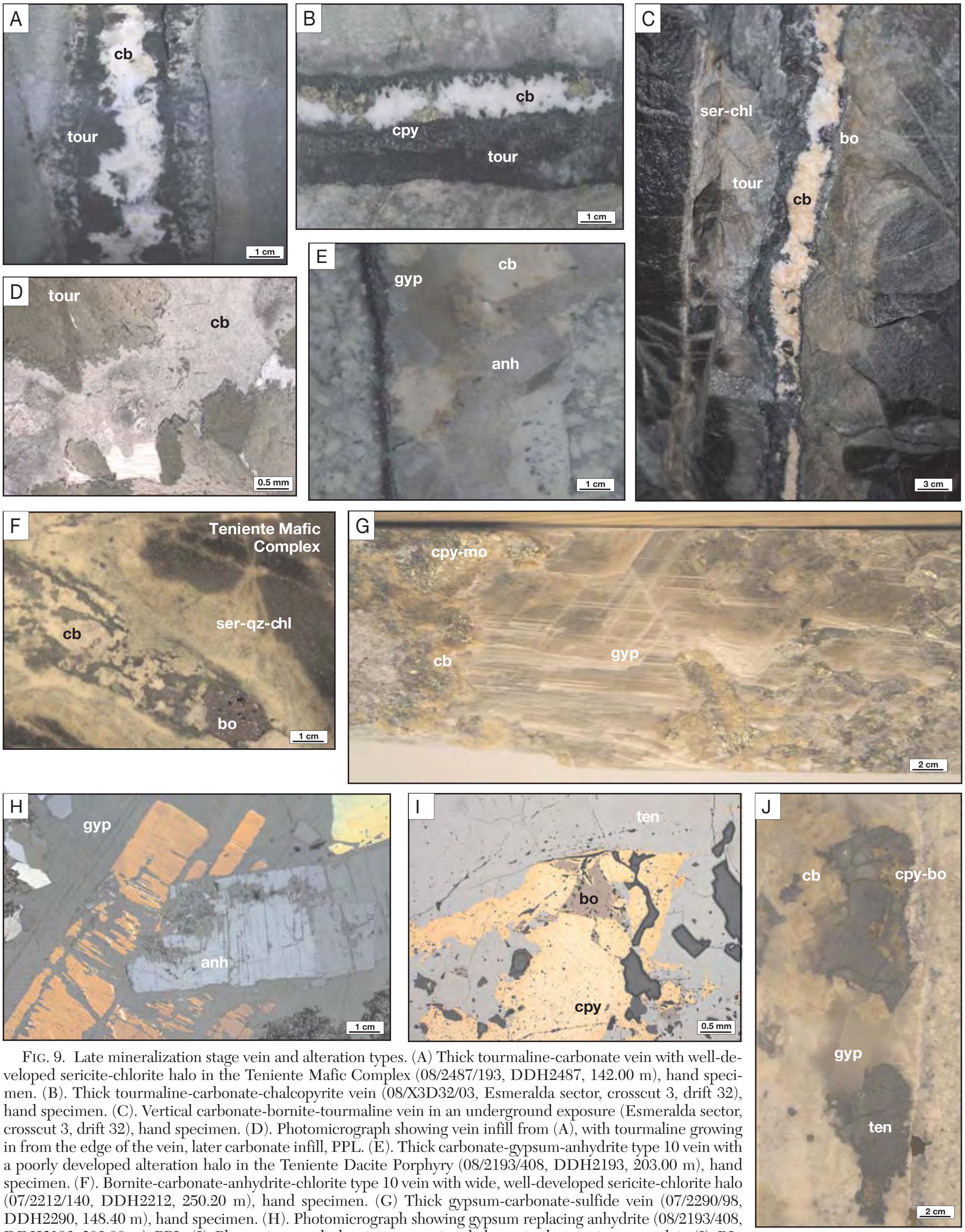

FIG. 9. Late mineralization stage vein and alteration types. (A) Thick tourmaline-carbonate vein with well-developed sericite-chlorite halo in the Teniente Mafic Complex (08/2487/193, DDH2487, 142.00 m), hand specimen. (B). Thick tourmaline-carbonate-chalcopyrite vein (08/X3D32/03, Esmeralda sector, crosscut 3, drift 32), hand specimen. (C). Vertical carbonate-bornite-tourmaline vein in an underground exposure (Esmeralda sector, crosscut 3, drift 32), hand specimen. (D). Photomicrograph showing vein infill from (A), with tourmaline growing in from the edge of the vein, later carbonate infill, PPL. (E). Thick carbonate-gypsum-anhydrite type 10 vein with a poorly developed alteration halo in the Teniente Dacite Porphyry (08/2193/408, DDH2193, 203.00 m), hand specimen. (F). Bornite-carbonate-anhydrite-chlorite type 10 vein with wide, well-developed sericite-chlorite halo (07/2212/140, DDH2212, 250.20 m), hand specimen. (G) Thick gypsum-carbonate-sulfide vein (07/2290/98, DDH2290, 148.40 m), hand specimen. (H). Photomicrograph showing gypsum replacing anhydrite (08/2193/408, DDH2193, 203.00 m), PPL. (I). Photomicrograph showing tennantite-chalcopyrite-bornite intergrowth in (J), RL. (J). Thick, gypsum-carbonate-sulfide vein with large tennantite crystals overgrowing and/or replacing chalcopyrite-bornite (08/2193/399, DDH2193, 181.00 m), hand specimen. Abbreviations: anh = anhydrite, bo = bornite, cb = carbonate, chl = chlorite, cpy = chalcopyrite, gyp = gypsum, mo = molybdenite, PPL = plane-polarized light, qz = quartz, RL = reflected light, ser = sericite, ten = tennantite, tour = tourmaline, XPL = cross-polarized light.

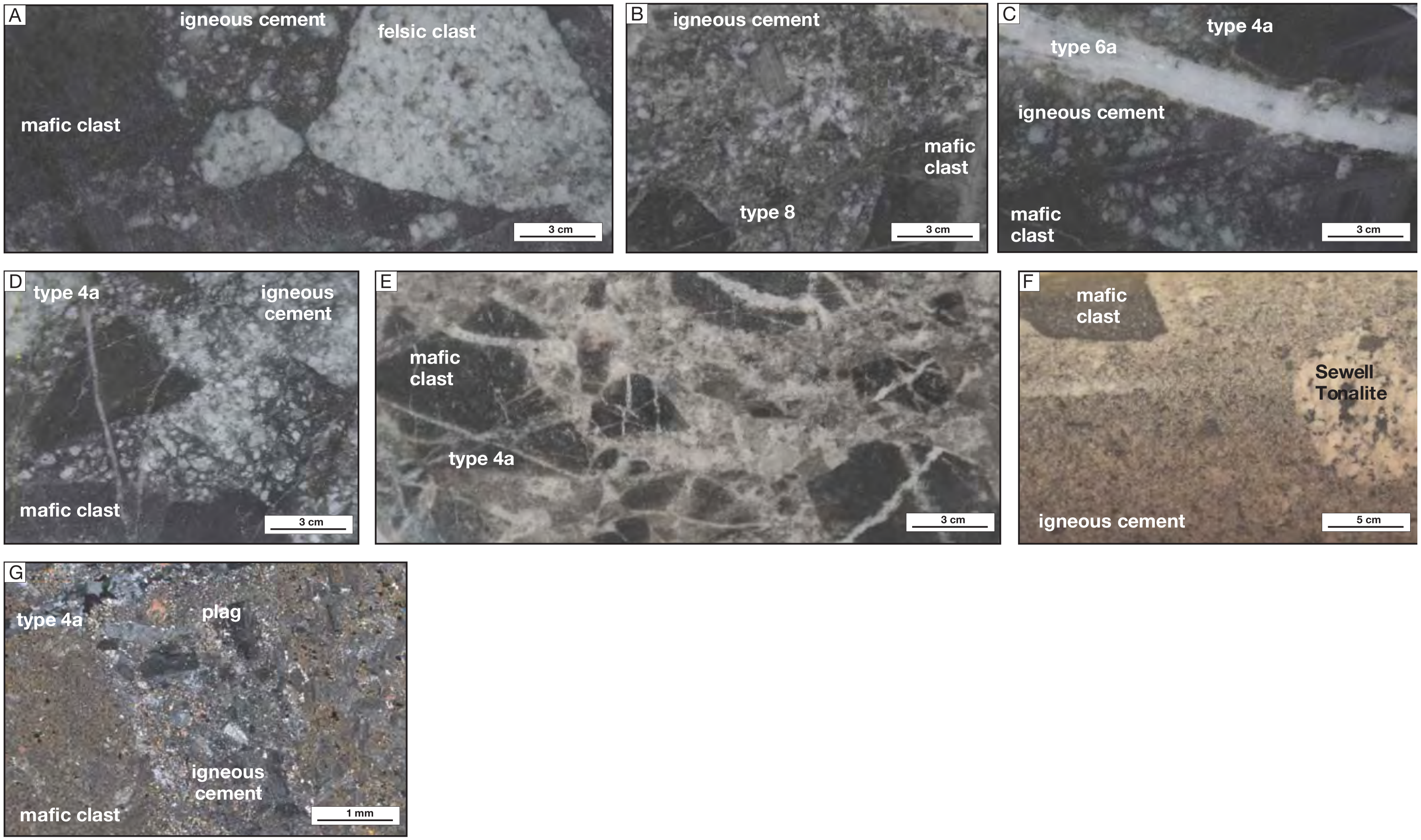

FIG. 10. Igneous breccia types observed at El Teniente. (A). Igneous breccia located at the margin of the Teniente Dacite Porphyry containing both Teniente Mafic Complex clasts and dacite clasts. Disseminated sulfides occur in both clasts and igneous matrix (08/1034/28, DDH1034, 111 ft), hand specimen. (B). Igneous breccia along the margin of the Southern Dacite Porphyry containing Teniente Mafic Complex clasts. Type 8 veins with sericitic halos cut both clasts and matrix (07/2327/159, DDH2327, 71.00 m), hand specimen. (C). Igneous breccia at depth spatially associated with the Teniente Dacite Porphyry cut by type 4a veins that are in turn cut by type 6a veins (08/1034/45, DDH1034, 1631 ft), hand specimen. (D). Igneous breccia cut by type 4a veins along the margin of the North-Central Dacite Porphyry (08/2240/632, DDH2240, 427.80 m), hand specimen. (E). Igneous breccia surrounding the Teniente Dacite Porphyry with terminated type 4a quartz-K-feldspar veins in mafic clasts (08/2452/596, DDH2459, 195.50m), hand specimen. (F). A-Porphyry igneous breccia containing mafic Teniente Mafic Complex clast and rounded Sewell Quartz Diorite clast (08/2487/310, DDH2487, 401.00 m), hand specimen. (G). Photomicrograph of igneous cement between Teniente Mafic Complex clasts and cross-cutting type 4a vein (08/2240/632, DDH2240, 427.80 m), XPL. Abbreviations: plag = plagioclase feldspar; PPL = plane-polarized light, XPL = cross-polarized light.

the two adjacent lithologic units between which the breccias are developed and, although both mafic and felsic clasts are present, mafic clasts are the dominant type. Many of these igneous breccias are cemented with a relatively dark-colored igneous matrix that is not readily identified in drill core or underground exposures due to a lack of contrast between the igneous cement, mafic clasts, and the Teniente Mafic Complex and can only be easily recognized where they contain felsic porphyry clasts. Consequently, these are difficult to map and their extent may be greater than is currently documented.

K-feldspar breccias

K-feldspar cemented breccias (Fig. 11A) were observed in this study only at deep levels in the A-Porphyry breccia complex. They are clast dominated, in situ to clast-rotated monomictic breccias, comprising subangular to subrounded clasts of the Sewell Quartz Diorite cemented by coarse-grained (up to 2 cm) K-feldspar, exhibiting microperthitic texture with intergrowths of albite (Table 5, Fig 11B). Rock flour is absent. The K-feldspar breccias are closely spatially associated with actinolite-, biotite- and anhydrite-dominated breccias but probably predate at least the biotite- and anhydrite-dominant facies as indicated by the occurrence of biotite-anhydrite-chalcopyrite precipitated in cracks in feldspar crystals (Fig. 11B). No copper or molybdenum sulfides appear to be contemporaneous with K-feldspar breccia cements.

Biotite breccias

In this study, well-developed biotite-cemented breccia was observed only adjacent to the A-Porphyry igneous breccia in the southeast of the deposit (Figs. 1, 11C). This is a matrix-supported, polymictic breccia containing subrounded to subangular clasts of both the Teniente Mafic Complex and the Sewell Quartz Diorite up to 10s of centimeters in diameter. The cement comprises coarse-grained (up to 3 cm) biotite that forms radiating plates and cockade textures (Fig. 11C-D), often intergrown with pyrite, chalcopyrite, and later anhydrite (Fig. 11E-F). Hydrothermal biotite in breccia cement contains higher MnO and lower FeO than igneous biotite phenocrysts in felsic host rocks (Table 3). Much of the sulfide is deposited with the anhydrite in open space between biotite crystals (e.g., Fig. 11E-F). Thin section petrography of this coarse biotite has revealed intergrowths of ferroan calcite (Fig. 11G) containing 0.3 to 0.5 wt percent MnO and 4 to 5 wt percent FeO. These intergrowths appear to be secondary and related to alteration of biotite to chlorite. Similar textures have also been observed within primary igneous biotite from the Sewell Quartz Diorite (Fig. 4C). Rock flour is absent. Biotite breccia occurs spatially associated with the upper portions of the A-Porphyry stock, above and enveloping igneous breccias.

Anhydrite breccias

Anhydrite breccias are associated with the margins of all the mineralized intrusions at El Teniente; notably, they are absent from the Sewell Quartz Diorite except adjacent to the A-Porphyry (Fig. 1). The contacts between breccia and intrusion on one side and local host rock on the other are gradational so that it is difficult to map a well-defined boundary in drill core or in underground exposure. These breccias are typically associated with the upper portions of the intrusions, forming above and surrounding igneous-cemented breccias and both igneous- and biotite-cemented breccias in the A-Porphyry. Anhydrite breccias range from clast to matrix supported and are polymictic, always containing millimeter- to tens of centimeter-scale, subangular to subrounded clasts of the Teniente Mafic Complex plus clasts of igneous breccia, Sewell Quartz Diorite, dacite finger porphyry or Teniente Dacite Porphyry, depending on their location (Fig. 11H). Clasts are cemented by coarse anhydrite-quartz ± sulfides-biotite-tourmaline (Fig. 11D, I-J). Early cements are dominated by biotite, with an inferred gradation from the biotite breccias described above. Later cements are dominated by anhydrite which may be intergrown with quartz. Chalcopyrite occurs intergrown with both biotite and anhydrite. Rock flour is absent. Specific mineral associations within the anhydrite

FIG. 11. Hydrothermal breccia types observed at El Teniente. (A). K-feldspar breccia with biotite-anhydrite-chalcopyrite developed along cracks (07/2290/114, DDH2290, 296.60 m), hand specimen. (B). Photomicrograph showing coarse K-feldspar from a K-feldspar breccia with microperthite texture and later anhydrite and sulfides along grain boundaries and within cracks (07/2290/114, DDH2290, 296.60 m), XPL. (C). Coarse biotite breccia from the A-Porphyry complex with Sewell Quartz Diorite clasts (1700E 40N level 2,163- Esmeralda Sector), hand specimen. (D). Anhydrite-biotite breccia from the A-Porphyry complex with Sewell Quartz Diorite clasts in igneous matrix (A-Porphyry) cut by type 4a veins that are in turn cut by anhydrite-biotite breccia cement (07/2290/104, DDH2290, 174.00 m), hand specimen. (E). Photomicrograph of a biotite-cemented breccia surrounding the A-Porphyry, showing anhydrite-chalcopyrite-quartz growth in open space between biotite crystals that contain secondary calcite laminae (08/2428/830, DDH2428, 212.00 m), XPL. (F). Photomicrograph of a biotite-cemented breccia surrounding the A-Porphyry, showing anhydrite-chalcopyrite growth in open space between biotite crystals, one of which is bent (08/2428/830, DDH2428, 212.00 m), XPL. (G). Biotite with secondary calcite (07/2290/104, DDH2290, 174.00 m), XPL. (H). Anhydrite breccia from adjacent to the North-Central Dacite Porphyry containing clasts of igneous breccia, Teniente Mafic Complex and dacite cut by type 8 veins, with type 4a veins truncated in mafic clasts (SITIO2 Geotechnical drill core, 1.50 m), hand specimen. (I). Anhydrite breccia containing Sewell Quartz Diorite clasts with truncated type 4a veins, cemented by anhydrite-chalcopyrite(-pyrite) with the sulfides partly cutting and/or replacing anhydrite (07/2305/44, DDH2305, 47.60 m), hand specimen. (J). Tourmaline-quartz-chalcopyrite breccia located south of the Braden Breccia Pipe containing sericitic altered felsic clasts cut by sulfides (08/532, Diablo Sector, south of drift 27), hand specimen. (K). Photomicrograph of (J) showing multiple generations of tourmaline growth. Early blocky tourmaline appears brecciated with later sprays of acicular tourmaline overgrown by quartz (08/532, Diablo Sector, south of drift 27), XPL. (L). Abundant, thin, diffuse-walled tourmaline veinlets with sericitic alteration halos in the A-Porphyry (08/2487/203, DDH2487, 159.85m), hand specimen. (M). Abundant, thin tourmaline veinlets in the North-Central Dacite Porphyry creating a vein-breccia texture (08/2196/766, DDH2196, 86.40 m), hand specimen. Abbreviations: anh = anhydrite, bt = biotite, cal = calcite, cpy = chalcopyrite, Kfsp = K-feldspar, PPL = plane-polarized light, qz = quartz, ser = sericite, tour = tourmaline, XPL = cross-polarized light.

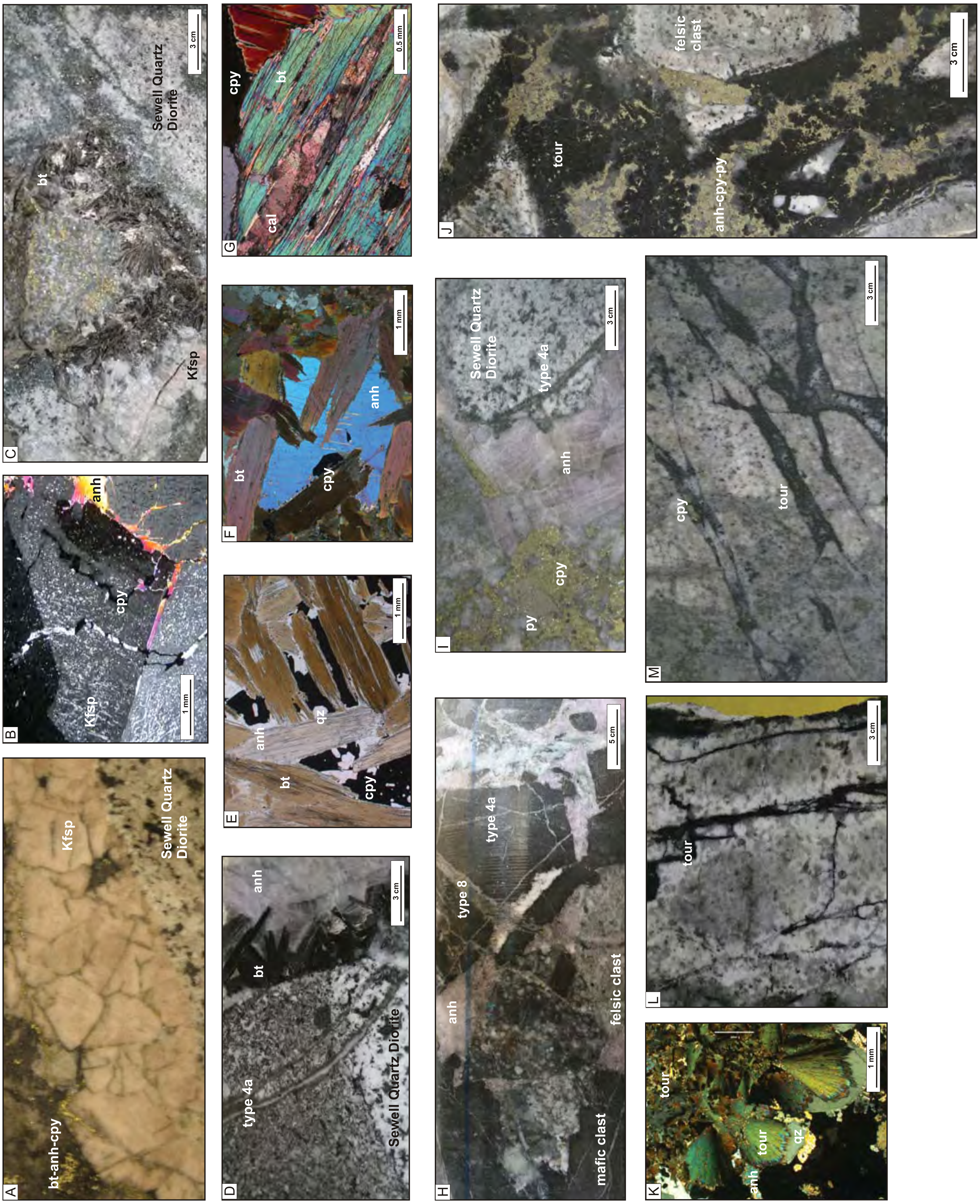
A
bt-anh-cpy
Kfsp
Sewell Quartz Diorite
B
Kfsp
cpy
anh
1 mm
C
Kfsp
bt
Sewell Quartz Diorite
3 cm
D
type 4a
bt
anh
Sewell Quartz Diorite
3 cm
E
bt
anh
qz
cpy
1 mm
F
bt
cpy
anh
1 mm
G
cal
bt
cpy
0.5 mm
H
anh
type 8
type 4a
mafic clast
felsic clast
5 cm
I
py
cpy
anh
type 4a
Sewell Quartz Diorite
3 cm
J
anh-cpy-py
tour
felsic clast
3 cm
K
anh
tour
qz
tour
1 mm
L
tour
3 cm
M
cpy
tour
3 cm

breccias depend on depth and location: for example, biotite is associated with the deeper parts of the A-Porphyry anhydrite breccia, whereas tourmaline occurs with anhydrite in a breccia complex to the south of the Braden Breccia Pipe (Figs. 1, 11J).

Tourmaline breccias

These are matrix-supported, polymictic breccias containing clasts of Teniente Mafic Complex and highly sericitized felsic rocks cemented by tourmaline-anhydrite-sulfides (Fig. 11J). They have been previously described above the A-Porphyry and were also seen associated with the Grueso Porphyry and as an independent breccia body occurring south of the Braden Breccia Pipe (Fig. 1). Clasts in tourmaline breccias are subangular and range from millimeters to tens of centimeters in size. Thin section petrography of a tourmaline breccia to the south of the Braden Breccia Pipe (Fig. 1) has identified two stages of tourmaline growth and brecciation: an early event associated with blocky, coarse tourmaline development and the formation of pyrite; and a second stage associated with the development of thin tourmaline needle overgrowths plus quartz, pyrite, and chalcopyrite (Fig. 10K). The outer halos of these breccias typically comprise locally abundant thin tourmaline veins, creating vein-crackle breccia textures (Fig. 10L-M).

Discussion

Vein chronology

The vein chronology presented here is broadly comparable to that seen in other porphyry-style copper deposits (e.g., Gustafson and Hunt, 1975). However, the classification includes an extra level of complexity with a total of ten vein types being defined and differs in some of the details of the mineral assemblages, in particular the abundance of biotite both within veins and as alteration halos within wall rocks. The classification is considered to represent the simplest that fully encompasses the range of veins observed but it is important to note that it incorporates a degree of arbitrary division where a continuum in vein compositions exists. It also involves a degree of interpretation, particularly in terms of conclusions about vein reactivation events that produce complex composite veins interpreted here to reflect separate veining episodes.

The general vein sequence begins with premineralization vein types (1–4) comprising biotite-K-feldspar-magnetite-actinolite ± minor quartz-anhydrite with biotite, plagioclase ± quartz alteration halos that contrast with the K-feldspar stable alteration that becomes more important in the main mineralization stage. These grade into gangue-dominated, main mineralization stage veins (5–6) composed of quartz-anhydrite ± minor sulfide with biotite or no alteration halos in the Teniente Mafic Complex and K-feldspar alteration in felsic hosts; these may have evolved into the later sulfide-dominated veins with no alteration halos (7) and finally sulfide-rich veins that are distinctive because of the first appearance of intense phyllic alteration halos (8). This is a characteristic that marks a progressive temporal and spatial change in fluid properties. The late mineralization stage veins are rather distinct with their tourmaline-carbonate-anhydrite-gypsum-sulfide assemblages and phyllic alteration halos.

Crosscutting relationships between the multiple vein types within the deposit were essential for defining the vein chronology. However, although the relative timing relationships between many vein types are clearly defined, there are veins for which no crosscutting relationships were observed, particularly within the premineralization stage (types 1 and 2; Fig. 12). Type 3 veins are well defined as an early vein type, being consistently overprinted by type 4a veins (e.g., Fig. 7I). Type 4a veins have not been observed to be cut by type 4b veins; however, these veins exhibit similar mineralogy and are separated spatially so the type 4b veins are interpreted to be the distal equivalents of type 4a veins. Similarly, type 4a veins have not been observed to be cut by type 5 anhydrite-dominated veins but they are consistently cut by anhydrite breccias throughout the deposit that are considered to be contemporaneous with type 5 veins (e.g., Figs. 11D, H, 13A). Type 6a quartz-dominated veins cut both anhydrite-dominated veins and anhydrite breccia cements (e.g., Fig. 8K). Reverse crosscutting relationships between type 5 and 6a veins were also observed, but these occurrences were isolated to drill core in and surrounding the Teniente Dacite Porphyry, consistent with its interpretation as a multiphase intrusion. Type 6b veins represent composite veins formed by reopening of type 6a veins during stage 7; examples were found where thin chalcopyrite-dominated veins (type 7a) cut, offset, and feed central sulfide seams within type 6a veins (e.g., Fig. 8G). Type 7 veins were also observed cutting and feeding sulfide seams within premineralization type 3 veins (Fig. 13B-C). Of the type 7 veins, molybdenite-rich veins formed earlier as shown by consistent crosscutting relationships with chalcopyrite veins (e.g., Fig. 8L). Also, type 6b veins often contain a thin molybdenite selvage with a central copper sulfide-dominated seam consistent with successive reopening during type 7a and b vein stages (e.g., Fig. 8G). Type 8 veins consistently cut premineralization stage veins and gangue-dominated main mineralization stage veins (Fig. 13D-E); however, no crosscutting

Offsetting vein (younger)

Offset vein (older) / Vein type	1	2	3	4a	4b	bt bx	5	anh bx	6a	6b	7a	7b	8	9	10
1															
2															
3			15	4	1		5	9	36	1	9		14		4
4a						2		20	5		4		4		1
4b									1		1				
bt bx									1	1	1		1		1
5									2		3		6		3
anh bx									7		3	1	10	3	3
6a							5		25		7	1	20		5
6b												3			
7a												2			
7b															
8													2		5
9															2
10															

FIG. 12. Matrix of observed vein crosscutting relationships. Veins are grouped according to their vein stage: premineralization (red); main mineralization (yellow); and late mineralization (blue). Abbreviations: anh = anhydrite, bt = biotite, bx = breccia.

relationships were observed between them and sulfide-dominated, main mineralization type 7 veins. This, combined with the abundance of stage 8 veins, extensive phyllic alteration above Teniente level 8 (1,983 m.a.s.l.), and a lack of evidence for sulfide remobilization during stage 8, suggests that type 7 and 8 veins are linked, with the type 7 veins being the deeper equivalents of type 8 veins. Although crosscutting relationships were only rarely observed between the two late mineralization stage vein types, tourmaline-bearing assemblages appear to be earlier, sometimes occurring as veins that have been reopened and replaced by a central carbonate seam (e.g., Fig. 9A-D).

Little to no copper sulfide deposition occurred during the premineralization vein stage: sulfides in these veins form a very small proportion of the total vein fill and can commonly be attributed to overprinting by later vein stages (e.g., Fig. 13B-C). The first significant primary sulfide deposition is interpreted to occur in vein types 5 and 6a, where chalcopyrite, pyrite, molybdenite, and bornite all occur although are minor components. The most important stage of introduction of copper and molybdenum is interpreted to have been via type 7 and 8 veins. These veins are generally thin (<5 mm), largely sulfide-dominant vein types that are very abundant within the deposit. Due to the thinness of the type 7 veins and weakness of the vein-wall contacts they are often observed as sulfide-coated broken surfaces both in drill core and underground exposures, hence their abundance may be greater than first impressions tend to suggest. In addition, some of the sulfide observed in earlier vein types can be attributed to overprinting by this stage (e.g., in the formation of composite type 6b veins; Fig. 8G). With the exception of a few areas in the mine, the late mineralization stage veins are not sufficiently abundant to significantly impact on Cu grade; the subeconomic grade (<0.5% Cu) mineralization of the Braden Breccia Pipe is probably related to the limited presence of veins of this type.

Several disparities exist between the vein classification proposed here and those presented in previous work (Fig. 14). The occurrence of veins in a range of host lithologic units can present problems when trying to correlate veins because of the variable alteration halos that may have formed. This is particularly true for late, main mineralization stage veins with phyllic halos (e.g., Fig. 13F-I) but also for the earlier type 5 veins. Careful examination of individual veins at the point where they transect lithologic contacts has helped to resolve this problem. Emphasis on different vein stages or the observation of unique vein types may also have occurred as a result of a specific spatial focus within the deposit; in this study, the increased number of vein types defined in the premineralization stage (Fig. 14) partly reflects observations made on deeper drilling not available to previous workers. A number of the remaining contradictions are probably due to the frequency of vein reopening that has produced composite vein types not easily assigned to a particular vein stage. This is particularly apparent when the revised chronology is compared to the El Teniente mine classification, which shows a repeated sequence of anhydrite- (V4 and V6), tourmaline- (V8 and V15), and magnetite- (V1 and V9) dominated veins which are here interpreted to reflect earlier vein and/or breccia types containing these phases that were overprinted during later vein stages, with the addition of sulfides and/or phyllic alteration halos.

Another important distinction is in the occurrence of anhydrite. Cannell et al. (2005) defined two distinct anhydrite-bearing stages representing anhydrite breccia and vein development associated with the A-Porphyry, and that associated with the probably slightly younger dacite finger porphyries and the Teniente Dacite Porphyry. Although these are likely to be distinct events temporally, within each intrusive complex (with the exception of multiple events associated with the Teniente Dacite Porphyry) only one paragenetic stage of anhydrite-bearing veins and breccias is observed. Consequently, the superimposition of an absolute temporal relationship of anhydrite formation on a deposit-wide relative chronology is considered to be misleading.

The new chronology presented here, similar to that of Cannell et al. (2005), shows only one sulfide-dominated vein type with a phyllic alteration halo. The three vein types presented in the mine geologists' classification show only minor variations in vein halos that do not appear to be consistent enough to warrant separate designations.

Lastly, the early tourmaline + phyllic alteration stage 1b vein type defined by Cannell et al. (2005) does not appear to have any equivalent in the new classification. Either these veins are related to the tourmaline breccia-related crackle veins described here or, perhaps more likely, they predate the development of the El Teniente mineralized system. Older (and younger) tourmaline breccia pipes with associated sericitic alteration are known elsewhere in the district, such as Olla Blanca to the northwest of El Teniente (Camus, 1975).

Breccia facies relationships and evolution

It is clear from extensive mapping and logging by mine geologists, supplemented by the work carried out for this study, that apart from the Sewell Quartz Diorite, each of the felsic-intermediate intrusions at El Teniente hosts its own breccia complex that is rather systematically zoned around the central intrusion. These complexes all show similar temporal evolution paths but it is important to note that, based on the available geochronology, they were not synchronous.

Crosscutting relationships indicate that the igneous breccias were always the earliest facies to form. These breccias are developed along the contact between the Teniente Mafic Complex and intrusive bodies as is typically observed in porphyry-type deposits (Sillitoe, 1985). They are mostly observed in the deeper parts of the breccia complexes, possibly reflecting an upward magmatic-hydrothermal transition and perhaps partly because of better preservation at depth where they have not been overprinted by subsequent breccia facies. The presence of felsic-intermediate clasts that have similar mineralogy and texture as the felsic-intermediate intrusive rocks they are spatially associated with indicates that they postdate at least partial crystallization of these intrusions. However, the fact that these bodies appear to form shells surrounding the pipelike intrusions strongly suggests that they are genetically linked to their emplacement and were probably formed by forceful intrusion—and possible subsequent retraction—of magmas with resulting entrainment and/or collapse of country-rock fragments and reworking of crystallized carapace material. The subrounded nature of some of the clasts implies a degree of transport and physical and/or chemical abrasion during formation.

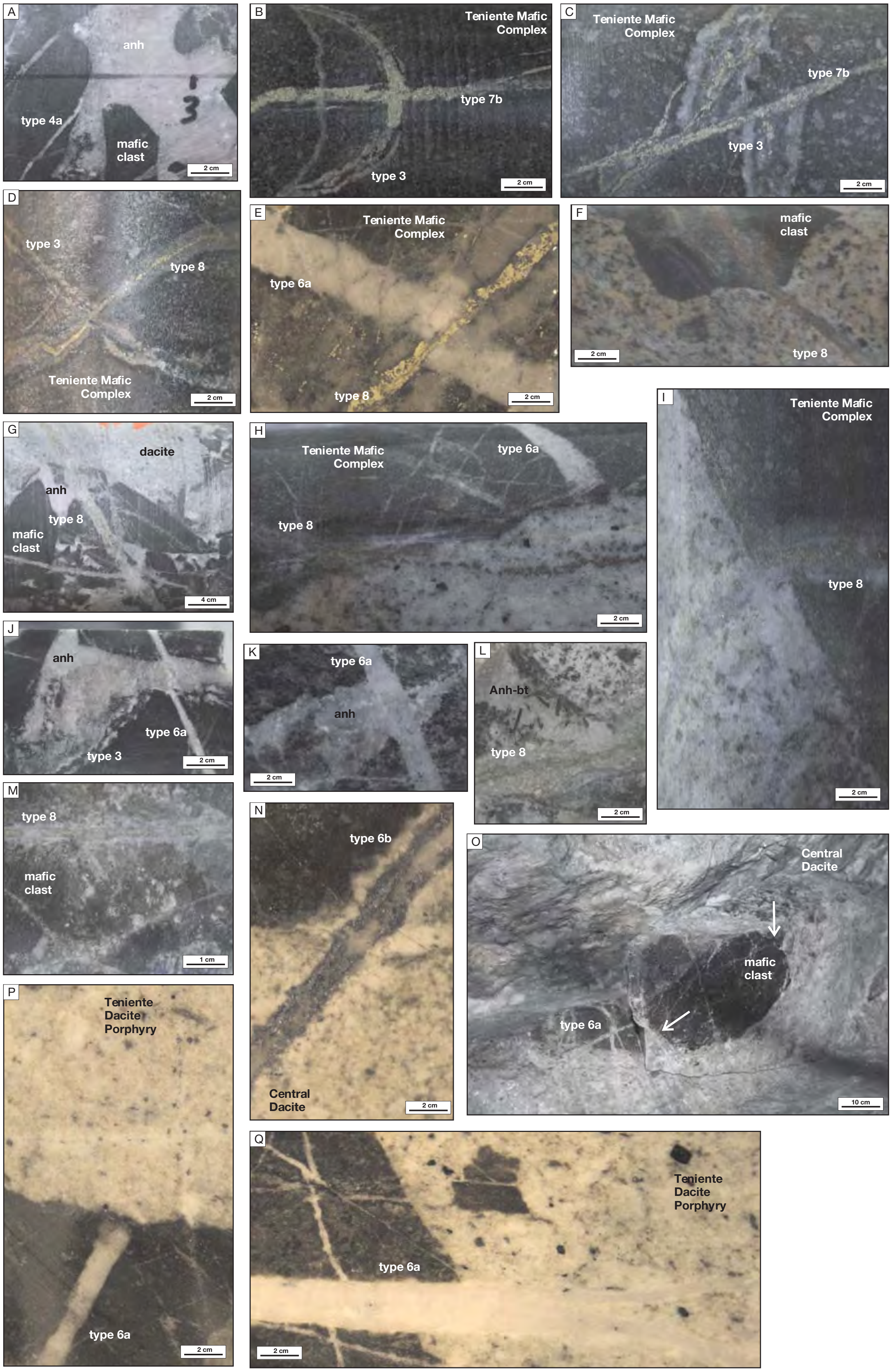

A
anh
type 4a
mafic clast
2 cm
B
Teniente Mafic Complex
type 7b
type 3
2 cm
C
Teniente Mafic Complex
type 7b
type 3
2 cm
D
type 3
type 8
Teniente Mafic Complex
2 cm
E
Teniente Mafic Complex
type 6a
type 8
2 cm
F
mafic clast
type 8
2 cm
G
dacite
anh
type 8
mafic clast
4 cm
H
Teniente Mafic Complex
type 6a
type 8
2 cm
I
Teniente Mafic Complex
type 8
2 cm
J
anh
type 6a
type 3
2 cm
K
type 6a
anh
2 cm
L
Anh-bt
type 8
2 cm
M
type 8
mafic clast
1 cm
N
type 6b
Central Dacite
2 cm
O
Central Dacite
mafic clast
type 6a
10 cm
P
Teniente Dacite Porphyry
type 6a
2 cm
Q
Teniente Dacite Porphyry
type 6a
2 cm

The igneous breccias are postdated by a series of breccias with cements of K-feldspar, biotite, anhydrite, and tourmaline that, with the notable exception of anhydrite, are typical of high-temperature magmatic-hydrothermal breccias associated with porphyry mineralization (Sillitoe, 1985). The deepest and earliest coarse K-feldspar-cemented breccias have only been observed to date in the A-Porphyry breccia complex. These contain little or no synchronous sulfide implying premineralization timing. In the A-Porphyry, these are overprinted and/or overlain by biotite- and anhydrite-cemented breccias with a gradation from more biotite dominant at depth to anhydrite dominant upward. Here, and in the dacite porphyry-associated breccia complexes, the anhydrite breccias contain clasts of Teniente Mafic Complex, felsic intrusive and igneous breccia (e.g. Fig. 11H), confirming that they developed later. The gradational outer contacts with the country rocks are typical of magmatic-hydrothermal breccias in porphyry systems (Sillitoe, 1985). Variable clast rounding is indicative of a degree of transport and/or chemical corrosion. Both biotite- and anhydrite-cemented breccias contain significant copper and molybdenum sulfides as cements, indicating onset of mineralization during formation of these early (within the life of the local system) but postintrusive breccias. Tourmaline breccias appear to form above, or independent of, other breccia types. They commonly contain abundant anhydrite and also significant copper and molybdenum sulfides. The subangular nature of the clasts suggests less transport.

Breccia-vein relationships

The occurrence of different clast types in breccias, terminated veins within clasts, and crosscutting veins were used to determine the relative timing of breccia facies within the new vein classification (Fig. 14).

Igneous breccias associated with the A-Porphyry and the dacite finger porphyries are cut by type 4a veins (e.g., Fig. 10D), indicating an early timing of these breccias within the hydrothermal evolution of each of these systems, consistent with their inferred synporphyry emplacement. Type 4a veins are the earliest veins that cut the A-Porphyry igneous breccia matrix indicating probable crystallization broadly synchronous with type 3 and 4 veins. One example of an igneous breccia, spatially associated with the Teniente Dacite Porphyry, contains mafic clasts with terminated type 4 veins (Fig. 10E). This suggests multistage development of this breccia, overlapping with type 4a veins, possibly linked to different phases of intrusion of the porphyry (Duarte, 2000; Rojas, 2003). Overall, the crosscutting evidence suggests that type 3 and 4 veins formed closest in space and time to the porphyry intrusions and should therefore represent the most primitive magmatic-hydrothermal fluids. The comparable mineral assemblages suggest these veins are genetically related to the K-feldspar and biotite-cemented breccias (Fig. 14).

Biotite-anhydrite breccias spatially associated with the A-Porphyry and anhydrite breccias associated with the North-Central Dacite Porphyry truncate type 4a veins (Fig. 11D, H-I) consistent with the breccia relationships that indicate these breccias are—at least partly—slightly younger than their spatially associated igneous breccias. These relationships also indicate that biotite-anhydrite breccias postdate some degree of crystallization and veining of spatially associated felsic-intermediate intrusions, at least at the level currently intersected by drilling and exposed in underground development. Type 6 quartz veins cut anhydrite breccias (Fig. 13J-K) and anhydrite veins (Fig. 8K), and igneous-, biotite- and anhydrite-cemented breccias are all cut by all vein stages from type 8 onward (e.g., Fig. 13L-M). These crosscutting relationships, together with

FIG. 13. Vein-breccia intrusion relationships. (A). Anhydrite breccia cement terminates premineralization type 4a veins, margin of the North-Central Dacite Porphyry (SITIO2 Geotechnical drill core, 3 m), hand specimen. (B). Main mineralization type 7b vein cuts premineralization type 3 vein (08/2487/177, DDH2487, 68 m), hand specimen. (C). Main mineralization type 7b vein cuts premineralization type 3 vein forming a central sulfide seam (08/2487/209, DDH2487, 172.90 m), hand specimen. (D) Premineralization type 3 vein cut by main mineralization type 8 vein (DDH2483, 183 m), hand specimen. (E). Main mineralization quartz-dominated type 6a vein cut and displaced by type 8 vein (07/2327/162, DDH2327, 135.50 m), hand specimen. (F). Main mineralization stage type 8 vein cuts Teniente Mafic Complex clast in Sewell Quartz Diorite. Note the change in halo across the contact (DDH2487, 296 m), hand specimen. (G). Anhydrite breccia with both mafic and felsic clasts cut by main mineralization type 8 vein proximal to the North-Central Dacite Porphyry. Note the slight change in halo width and color between mafic and felsic hosts (SITIO2 Geotechnical drill core, 2.50 m), hand specimen. (H). Teniente Dacite Porphyry-Teniente Mafic Complex contact cut by main mineralization stage type 8 vein and terminating type 6a vein. Again note change in halo across contact (08/2193/382, DDH2193, 115.15 m), hand specimen. (I). Sewell Quartz Diorite-Teniente Mafic Complex contact cut by main mineralization stage type 8 vein, with halo variation across contact (08/2487/291, DDH2487, 291.70 m), hand specimen. (J). Quartz type 6a vein cuts anhydrite breccia associated with the Teniente Dacite Porphyry. Anhydrite breccia cement terminates type 3 vein (08/2193/376, DDH2193, 92.80 m), hand specimen. (K). Quartz type 6a vein cuts anhydrite breccia associated with the Teniente Dacite Porphyry (08/1873/509, DDH1873, 518 ft), hand specimen. (L). Main mineralization stage type 8 vein cuts biotite-anhydrite breccia associated with the A-Porphyry (08/2428/806, DDH2428, 186.80 m), hand specimen. (M). Igneous-cemented breccia associated with the North-Central Dacite Porphyry cut by main mineralization stage type 8 vein (08/2215/714, DDH2215, 70.10 m), hand specimen. (N). Teniente Mafic Complex-Central Dacite Porphyry contact cut by molybdenite-rich type 7a vein with K-feldspar halo particularly well-developed in the Teniente Mafic Complex (07/2512/130, DDH2512, 88.80 m), hand specimen. (O). Underground exposure showing the Central Dacite Porphyry terminating Teniente Mafic Complex-hosted, premineralization type 4 veins (arrowed) but cut by later, main mineralization type 7a veins (Esmeralda Sector), hand specimen. (P). Teniente Mafic Complex-Teniente Dacite Porphyry contact truncating a main mineralization, bornite-bearing type 7a vein in the Teniente Mafic Complex. Thin, type 7 veins containing bornite cut the contact (07/2212/141, DDH2212, 255.60 m), hand specimen. (Q). Teniente Mafic Complex-Teniente Dacite Porphyry contact terminating type 4a veins in Teniente Mafic Complex and cut by a main mineralization, bornite-bearing type 6a vein (07/2212/143, DDH2212, 261.00 m), hand specimen. Abbreviations: bt = biotite, anh = anhydrite.

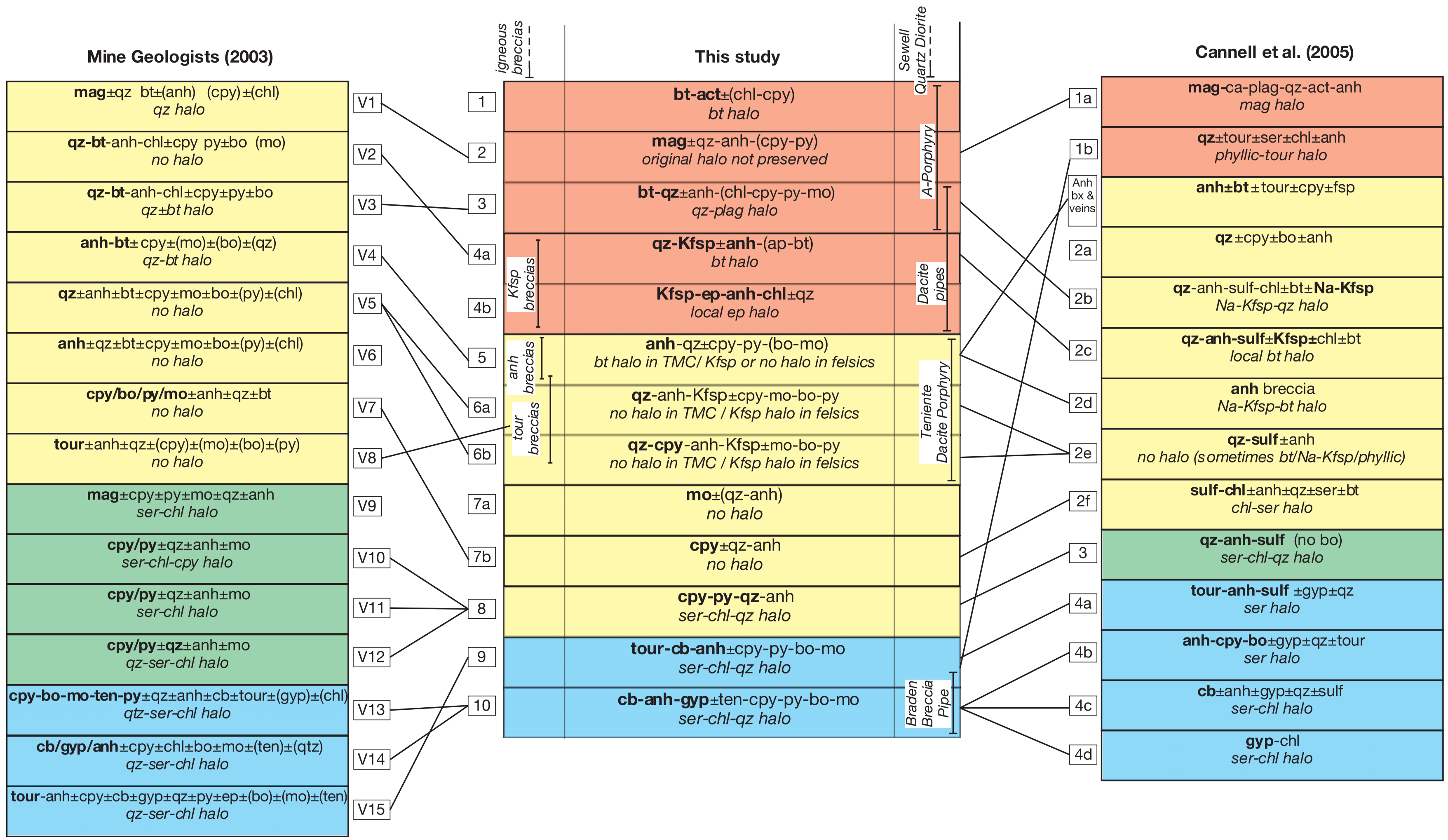

FIG. 14. Vein classification correlation, showing vein terminologies of El Teniente mine geologists (2003) and Cannell et al. (2005) compared with the new classification presented in this study. Veins are grouped into alteration stages as defined by previous authors and redefined here: premineralization (red); late magmatic and/or principal hydrothermal (= main mineralization; yellow); and late hydrothermal (= late mineralization; blue). The late magmatic stage from El Teniente mine geologists (2003) and Cannell et al. (2005) is shown in green. The relative timing of each intrusion and breccia type within the locally developed vein sequence is indicated. Note that this does not imply a single, deposit-wide vein chronology. Abbreviations as for Figures 7 to 10, plus Na-Kfsp = sodic plagioclase and K-feldspar, sulf = sulfides.

common mineral assemblages, clearly link the development of the biotite-anhydrite breccias to the initiation of the main mineralization stage dominated by type 5 anhydrite(+biotite selvage) veins. Anhydrite-biotite breccias and their associated veins appear to mark a key stage in the evolution of all the mineralized intrusion-centered systems at El Teniente.

The position of jigsaw-fit tourmaline breccias as caps on top of breccia complexes (e.g., associated with the A-Porphyry and Grueso Porphyry), the observation of probably contemporaneous tourmaline crackle-breccia veins cutting anhydrite breccia cement, and the fact that no crosscutting veins have been observed in tourmaline breccias, suggest that these breccias are the last to develop. The occurrence of tourmaline breccias and veins independent of other magmatic-hydrothermal breccia facies, such as the Tourmaline Marginal Breccia, the late type 9 tourmaline veins, and other tourmaline breccias in the district, indicates they can form by a separate mechanism and may not necessarily represent the endpoint of localized intrusion breccia-complex evolution.

Late mineralization stage carbonate-anhydrite-gypsum–bearing veins are concentrically orientated around the Braden Breccia Pipe (Cannell et al., 2005). This, plus the distinctive tourmaline-association that is also observed in the Tourmaline Marginal Breccia of the pipe, suggests that they are likely to have been formed at the same time. The Braden Breccia central facies of the pipe is only cut by veins from the late mineralization stage and contains no earlier vein types except as truncated veins in clasts, indicating that type 9 and 10 veins formed during and/or after pipe development and after all the mineralized complexes in the deposit. This is consistent with existing geochronology (Fig. 3).

Intrusion-vein relationships

The Sewell Quartz Diorite is cut by all vein types in the deposit including premineralization veins (e.g., early biotite-actinolite and early magnetite veins; Fig. 7A-B), indicating a premineralization timing for this intrusion. Given that no premineralization veins were observed in any of the younger felsic-intermediate intrusions, it is possible that there is a genetic link between these veins, the widespread magnetite ± biotite alteration (Cannell, 2004) and the intrusion of the Sewell Quartz Diorite, although premineralization veining and alteration ahead of younger rising magmas (e.g. the A-Porphyry, small dacite porphyries, and the Teniente Dacite Porphyry) cannot be excluded.

The North-Central Dacite Porphyry and the Central Dacite Porphyry truncate type 4a veins and are cut by anhydrite breccias (which also cut type 4a veins; Fig. 13A) and by type 5 and 6 veins (Fig. 13N-O). This places their relative intrusion age, at least at the currently accessible levels of exposure, between vein types 4 and 5.

The Teniente Dacite Porphyry cuts and is cut by type 6 veins (Fig. 13P-Q), indicating that it probably contains multiple intrusive phases as suggested by the multiphase igneous breccia associated with it noted earlier and by previous work (e.g., Rojas, 2003). This makes it difficult to assign a relative emplacement age although it is likely to be post-type 4 veins based on the igneous breccia relationships noted above, and partly post-type 6 veins, at least for the later phase(s) of emplacement. This sets it apart from the dacite finger porphyries that always appear to predate type 6 veins (e.g., Fig. 13N-O) and the A-Porphyry that predates type 4 veins (e.g., Fig. 11D).

Because of the crosscutting relationships between intrusions, breccias, and veining described, it is considered highly unlikely that the differences in relative emplacement ages can be accounted for by different timings of porphyry intrusions within a deposit-wide vein chronology. Rather, it is considered that this reflects different exposure levels in the complexes that preserve contrasting stages of evolution. The A-porphyry appears to preserve the closest spatial and temporal relationship between magmatic crystallization and release of the earliest magmatic-hydrothermal fluids, with later vein types superimposed in a retrograde fashion. It is the only igneous breccia that does not contain clasts of a local preexisting porphyritic intrusion. In contrast, the dacite porphyries can be inferred to have overprinted the earliest magmatic-hydrothermal vein types in their vicinity, perhaps by continued upward magma migration (including the formation of igneous breccias), until after vein stage 5 (or stage 6 for the Teniente Dacite Porphyry) when retrograde overprinting of the earlier breccia and vein facies began. Such a difference in behavior could be linked to the different composition and volatile content, and consequent emplacement and crystallization behavior, of the different intrusions.

Implications for the genesis of El Teniente

The geologic relationships described and previous geochronology (Fig. 3) lead to the conclusion that the El Teniente system comprises multiple intrusive centers, each of which produced its own breccia complex, typically in the upper portion of the intrusive body, during emplacement. These breccias are of significant spatial extent with respect to the dimensions of the host intrusion (Fig. 6).

Copper-grade maps clearly show that high-grade mineralization is spatially related to the intrusive-breccia complexes (Fig. 15) and it can be argued that the wide eastern zone of mineralization that makes up the Esmeralda sector of the mine is largely controlled by the multiple dacite intrusive-breccia complexes. In contrast, molybdenum forms a rather distinctive grade zonation concentric to the Braden Breccia Pipe above ~2,000 m.a.s.l. (Fig. 15) that clearly overprints the Teniente Dacite Porphyry; this likely indicates remobilization and/or addition of molybdenite (via late mineralization type 9 and 10 veins) during the formation of the Braden Breccia Pipe. Unfortunately, none of the dated molybdenite samples (Fig. 15) are located within this halo to test this interpretation. Relict molybdenum highs associated with the A-Porphyry, the Central Dacite Porphyry, and the North-Central Dacite Porphyry are clearly visible on the edges of the inferred remobilized halo and at greater depths (Fig. 15), suggesting that primary molybdenum introduction was associated with each of these intrusion-breccia complexes, similar to copper. Notably, the oldest Re-Os ages were obtained from samples spatially associated with the earliest synmineralization intrusion, the A-Porphyry, which is also the most distal from the Braden Breccia Pipe. An association between high-grade mineralization and breccia bodies is a characteristic feature of many porphyry systems. To date, there is no evidence to suggest that these breccia bodies extend to significant depth (Fig. 6)

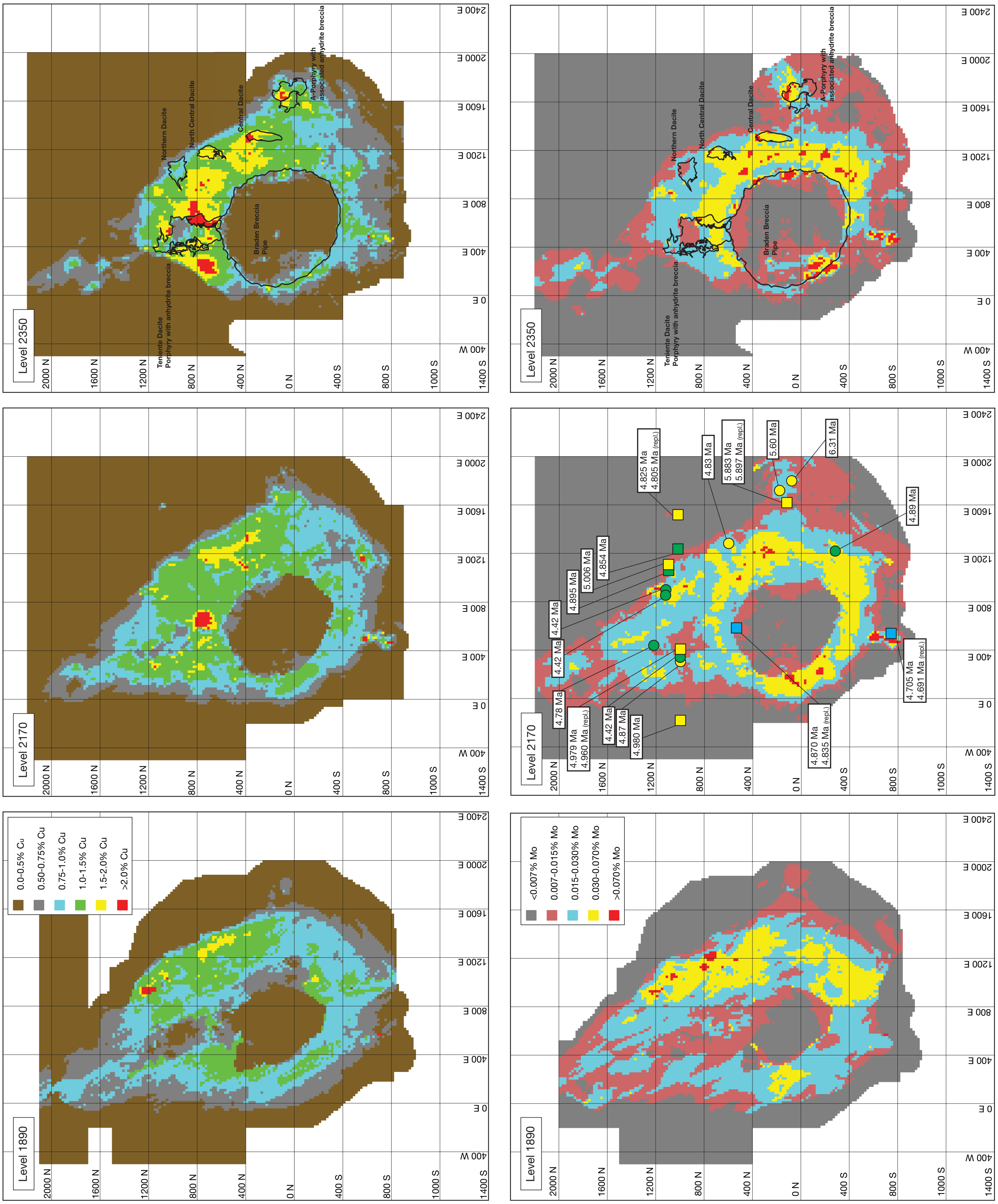

Level 2350
Level 2170
Level 1890
0.0-0.5% Cu
0.50-0.75% Cu
0.75-1.0% Cu
1.0-1.5% Cu
1.5-2.0% Cu
>2.0% Cu
<0.007% Mo
0.007-0.015% Mo
0.015-0.030% Mo
0.030-0.070% Mo
>0.070% Mo
Northern Dacite
North Central Dacite
Central Dacite
A-Porphyry with associated anhydrite breccia
Braden Breccia Pipe
Teniente Dacite Porphyry with anhydrite breccia
4.825 Ma
4.805 Ma (repl.)
4.83 Ma
5.883 Ma
5.897 Ma (repl.)
5.60 Ma
6.31 Ma
4.89 Ma
4.854 Ma
5.006 Ma
4.895 Ma
4.42 Ma
4.42 Ma
4.78 Ma
4.979 Ma
4.960 Ma (repl.)
4.42 Ma
4.87 Ma
4.980 Ma
4.870 Ma
4.835 Ma (repl.)
4.705 Ma
4.691 Ma (repl.)
2000 N
1600 N
1200 N
800 N
400 N
0 N
400 S
800 S
1000 S
1400 S
400 W
0 E
400 E
800 E
1200 E
1600 E
2000 E
2400 E

and that they predate and were relatively passively intruded by felsic intrusions as suggested by Skewes et al. (2002).

Although these breccias are important hosts of high-grade ore, over 80 percent of mineralization at El Teniente is hosted by the Teniente Mafic Complex (Camus, 1975; Cannell, 2004), mostly within stockworks composed of the multiple vein types described here. It is considered probable that vein types 3 to 5 represent a vein halo to the breccias and are equivalent to the K-feldspar, biotite, and anhydrite breccia facies, respectively. Brecciation can be linked to explosive degassing of volatile-rich magmas from the upper parts of the intrusions during their emplacement. Subsequent quartz-dominant vein types are particularly abundant at the margins of the felsic-intermediate intrusions and are interpreted as reflecting the progressive release of silica-rich magmatic-hydrothermal fluids from a deepening locus of magmatic volatile phase separation within each magma conduit, relatively soon after their intrusion to the current level of exposure. Even where breccias do not occur, vein abundances remain highest at the margins of the felsic-intermediate intrusive bodies (Cannell et al., 2005; this study), consistent with such a channeling of fluids from greater depths. Assay data show that vein abundance correlates with elevated grade across some of these contact zones (Fig. 16) forming the typical "ore shell" geometry characteristic of many porphyry copper deposits (Lowell and Guilbert, 1970).

The intrusion-breccia-veining relationships can be synthesized into a model for the evolution of individual complexes within the El Teniente deposit (Fig. 17), consistent with the multistage mineralization interpretation based on geochronology presented by Maksaev et al. (2004). Although a relatively consistent vein paragenesis can be defined for the deposit as a whole—typical of porphyry deposits elsewhere (Gustafson and Hunt, 1975; Seedorff and Einaudi, 2004; Seedorff et al., 2005)—it is unlikely that this reflects a single, deposit-wide evolution as implicitly or explicitly stated in previous studies (Cannell et al., 2005; Klemm et al., 2007). As concluded for El Salvador, the mineralization (vein) types described "are not necessarily time lines but rather parts of an evolving sequence which may be repeated" (Gustafson and Quiroga, 1995, p. 9). At El Teniente, a distinction can be made between vein types 1 and 2, which represent "prograde" veins formed, possibly deposit wide, prior to emplacement of intrusion-breccia complexes, vein types 3 to 8, which are interpreted to reflect the repeated cycle of thermal peak to retrograde fluid release associated with the emplacement of each mineralized intrusive complex, and vein types 9 and 10 that represent a single event linked to the emplacement of the Braden Breccia Pipe. The magmatic-hydrothermal transitions documented in these complexes indicate separate and localized pulses of hydrothermal activity which followed rather similar evolution paths. Although still controversial, existing geochronology suggests that these episodic events spanned more than 1.5 m.y. (Fig. 3) with a northerly migration of the locus of generally increasingly felsic magmatism.

In this model, the general lack of overprinting of later stage veins within earlier intrusive complexes by earlier stage veins in later complexes can be accounted for by the vertically elongate aspect ratio of the complexes, their spacing, and similar level of emplacement, which mean that such overprinting is likely to be uncommon (Fig. 17), except for the most distal vein types, such as type 8. Even for these veins, they are most likely to crosscut other type 8 veins so that a reverse crosscutting relationship would not be recognized. An exception is within the Teniente Dacite Porphyry where multiple, subjacent intrusive phases are inferred and where reverse crosscutting relationships (e.g., type 6 veins cut by type 5) are observed. Also, the overprinting of type 1 and 2 veins that are associated with biotite-actinolite-magnetite assemblages (inferred to have formed either related to the Sewell Quartz Diorite or above and distal to, rising source magmas) by later veins linked to the formation of the A-Porphyry complex can be regarded as a prograde overprinting relationship.

The geologic evidence documented here provides convincing evidence for a close genetic relationship between emplacement of shallow-level, felsic-intermediate pipelike intrusions and the development of igneous and mineralized magmatic-hydrothermal breccias along their margins and at their apices as has long been proposed at El Teniente (e.g., Camus, 1975). Crosscutting evidence clearly shows that the breccias at least partly overprint their associated intrusions rather than being intruded by them contrary to previous suggestions (e.g., Skewes et al., 2005). El Teniente thus represents a nested but otherwise rather typical porphyry Cu-Mo system, unusual only because the Teniente Mafic Complex provided a highly effective fractured and chemical trap for deposition of sulfides and because successive intrusive pulses were all well mineralized without barren, intermineral porphyries.

Conclusions

A revised classification of vein types at El Teniente incorporates 13 vein types that can be divided into three main stages: (1) premineralization biotite and/or K-feldspar ± quartz-anhydrite-albite-magnetite-actinolite-epidote veins that formed prior to emplacement of mineralized intrusions and breccias, possibly associated with the Sewell Quartz Diorite; (2) main mineralization stage veins that grade from gangue-dominated quartz-anhydrite veins ± potassic alteration halos into sulfide-dominated veins with phyllic alteration halos that are spatially associated with intrusion-related

Fig 15. Copper- and molybdenum-grade maps from three levels (m.a.s.l.) at El Teniente (provided by CODELCO Chile Division El Teniente), with outline geology overlain on both copper and molybdenum level 2,350 m maps. Molybdenum grade map at level 2,170 m shows the position of Re-Os dated molybdenite samples. Circles: data from Maksaev et al. (2004). Squares: data from Cannell (2004). Symbols are colored according to inferred ore stage (see Fig. 14) based on sample descriptions given by Maksaev et al. (2004) and Cannell (2004). Note the concentric molybdenum halo around the Braden Breccia Pipe in the upper levels and the shift to molybdenum localization around dacite finger porphyries at greater depth. Also note that a molybdenum low is associated with the Teniente Dacite Porphyry. Copper is concentrated proximal to the Teniente Dacite Porphyry at shallower levels but is localized around the dacite porphyries and the A-porphyry at depth.

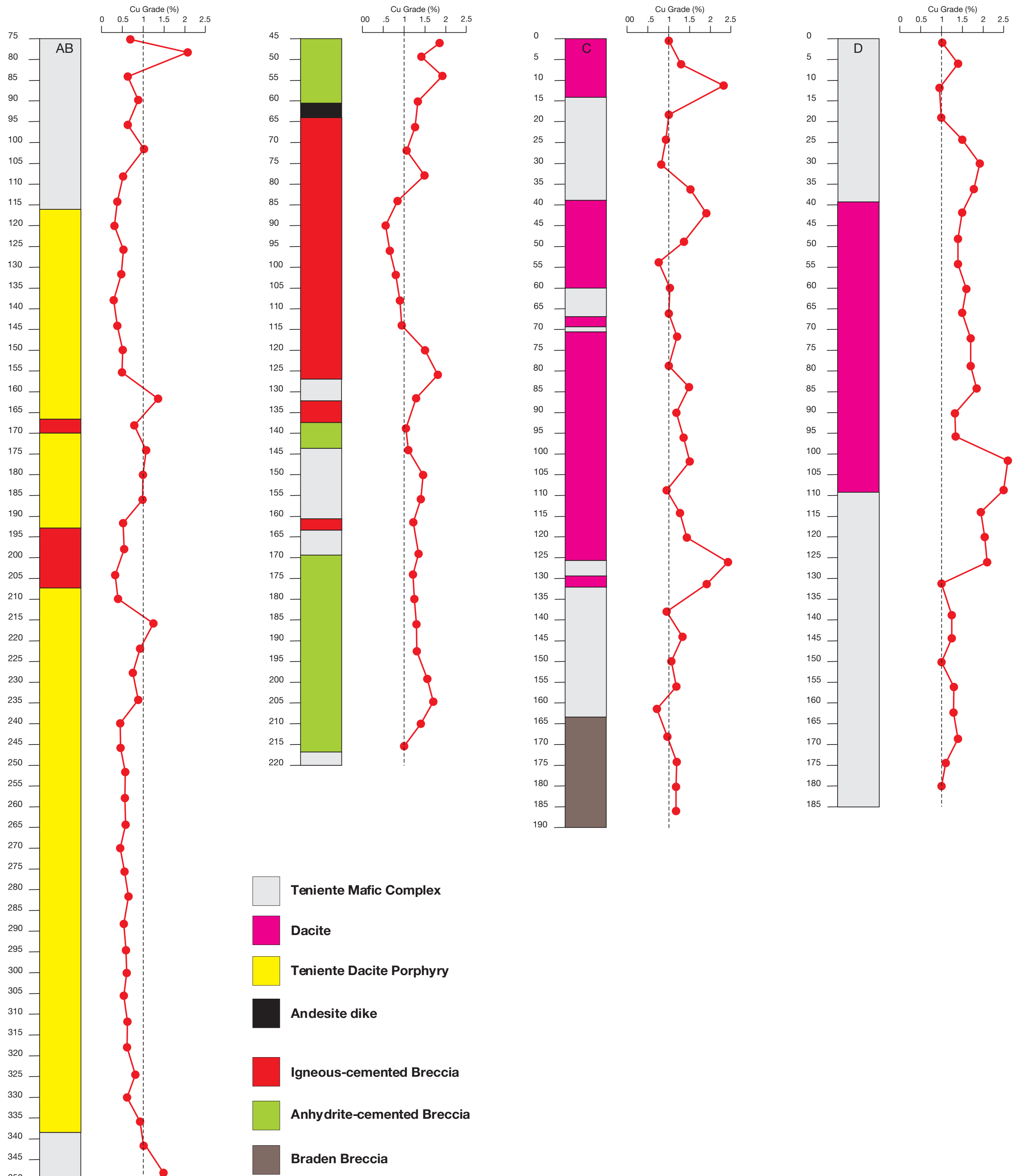

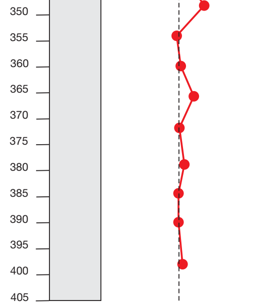

Fig 16. Representative examples of drill core logs from this study illustrating grade-lithology associations. (A). DDH2193 (Teniente Dacite Porphyry intersection). Note relatively low grade within the intrusion and elevated grade at contacts. (B). DDH2305 (A-Porphyry intersection). Note moderate grades within the A-Porphyry igneous breccia and high grades in surrounding anhydrite breccias. (C). DDH2327 (Southern Dacite Porphyry intersection). Note high grades within dacite and kicks at contacts. (D). DDH2417 (Central Dacite Porphyry intersection). Note very high grades within dacite and extremely high grades at contacts. Data courtesy of CODELCO División El Teniente.

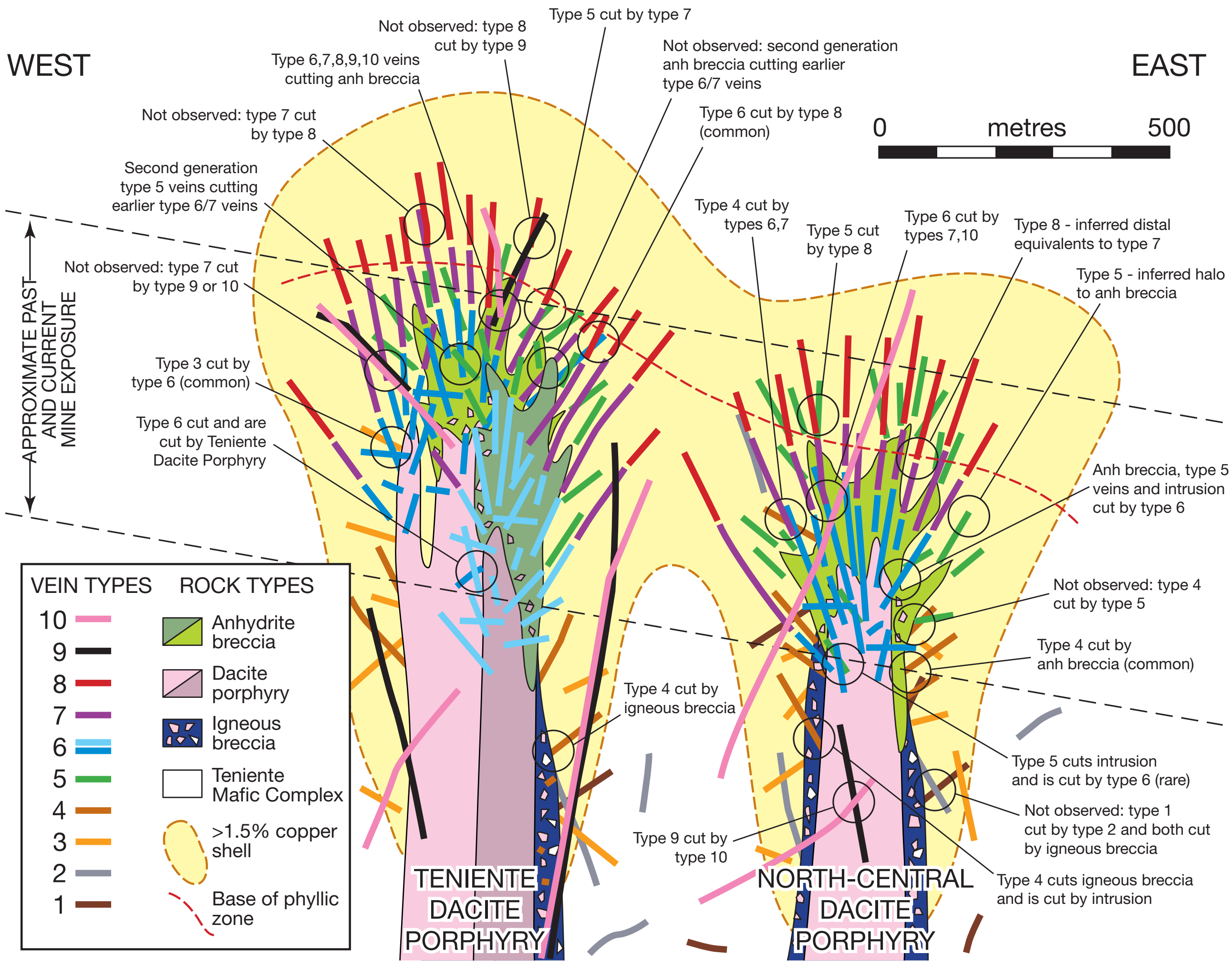

Fig 17. Schematic model for formation of nested porphyry and porphyry-related breccia complexes at El Teniente based loosely on geology along section line 700N (Figs. 1, 6) and back-rotated 10° to the east to remove the effect of postmineralization tilting. Intrusion, breccias, and vein relationships are shown: observed crosscutting relationships and expected (but not observed) relationships are highlighted. Note dipping base of phyllic zone related to emplacement depth of porphyries, predominance of type 6 veins at intrusion apices, and increasing relative importance of type 1 to 4 veins with depth. Mineralized halos around the two complexes shown merge to produce a continuous high-grade (>1.5% Cu) region in the upper levels but separated into individual root zones at depth. Because of its emplacement level, mineralization associated with the Teniente Dacite Porphyry predominates at shallower depths, whereas that associated with the apices of the dacite finger porphyries farther east becomes increasingly important at greater depths (see Fig. 15). Abbreviations: anh = anhydrite.

breccia complexes; and (3) late mineralization stage veins containing sulfosalts that are related to the emplacement of the Braden Breccia Pipe. Copper-molybdenum mineralization is intimately associated with the sequential intrusion of felsic-intermediate finger porphyries that developed multistage breccia complexes at their apices, together with surrounding vein halos. With the exception of minor tourmaline breccia pipes, breccia development did not occur prior to, or independent of, the emplacement of these intrusions. Multiple such events occurred at El Teniente, beginning with the intrusion of the A-Porphyry, through multiple dacite porphyry intrusions and terminating with the formation of the Braden Breccia Pipe, an explosive diatreme event which may have breached the surface, remobilized some preexisting mineralization, and effectively terminated ore formation. The emplacement of multiple nested porphyries within a relatively small host-rock volume created overlapping mineralized envelopes which acted to increase grade in the overlap zones. It is inferred that a long-lived underlying magma chamber that evolved to more felsic compositions through time and structural focusing of intrusions were key underlying controls of this evolution.

Acknowledgments

We would like to thank the members of the Superintendencia de Geología of the El Teniente mine, particularly Patricio Zuñiga, for granting access to the mine and allowing publication of this study. David Benado, Miguel Letelier, Roberto González, Juan Carlos Roa, Rodrigo Morel, and Ricardo Floody provided assistance, guidance, and useful discussions and debate. Thanks to the Natural History Museum, London, particularly Anton Kearsley, John Spratt, Terry Williams, Tony Wighton, Catherine Unsworth, and Stanislav

Strekopytov, and to CODES, particularly Karsten Göemann, for SEM laboratory support. Simon Stephens at CODES assisted with sample preparation. Funding for this project was obtained from multiple sources, including Imperial College London Janet Watson Scholarship, the Society of Economic Geologists Hugh McKinstry Student Research Grant and Graduate Student Fellowship, CODES, University of Tasmania, the Institute of Materials, Minerals and Mining G Vernon Hobson Bequest and Edgar Pam Fellowships, the Geological Society of London Elspeth Matthews Grant, the University of London Central Research Fund, the UK Resource Centre for Women Student Travel Bursary, and the Mineralogical Society Postgraduate Travel Bursary. We are grateful to Victor Maksaev for his invaluable criticisms of an initial draft of this manuscript and Jeremy Richards and an anonymous referee for their constructive comments.

REFERENCES

Cahill, T., and Isaacs, B., 1992, Seismicity and shape of the subducted Nazca plate: Journal of Geophysical Research, v. 97, p. 503–529.

Camus, F., 1975, Geology of the El Teniente orebody with emphasis on wall-rock alteration: ECONOMIC GEOLOGY, v. 70, p. 1341–1372.

Camus, F., 2003, Geología de los Systemas Porfíricos en los Andes de Chile: Santiago, Chile: Servicio Nacional de Geología y Minería, 267 p.

Cannell, J., 2004, El Teniente porphyry copper-molybdenum deposit, central Chile: Unpublished Ph.D. thesis, Hobart, Australia, University of Tasmania, 299 p.

Cannell, J., Cooke, D.R., Walshe, J.L., and Stein, H., 2005, Geology, mineralization, alteration, and structural evolution of the El Teniente porphyry Cu-Mo deposit: ECONOMIC GEOLOGY, v. 100, p. 979–1003.

——2007, Geology, mineralization, alteration and structural evolution of the El Teniente porphyry Cu-Mo deposit—a reply: ECONOMIC GEOLOGY, v. 102, p. 1171–1180.

Charrier, R., Baeza, O., Elgueta, S., Flynn, J.J., Gans, P., Kay, S.M., Muñoz, N., Wyss, A.R., and Zurita, E., 2002, Evidence for Cenozoic extensional basin development and tectonic inversion south of the flat-slab segment, southern central Andes, Chile (33º-36ºS): Journal of South American Earth Sciences, v. 15, p. 117–139.

Clark, A.H., Farrar, E., Camus, F., and Quirt, S., 1983, K-Ar age data for the El Teniente porphyry copper deposit, central Chile: ECONOMIC GEOLOGY, v. 78, p. 1003–1006.

Cooke, D.R., Hollings, P., and Walshe, J.L., 2005, Giant porphyry deposits: Characteristics, distribution, and tectonic controls: ECONOMIC GEOLOGY, v. 100, p. 801–818.

Cuadra, P.C., 1986, Geochronologia K-Ar del yacimiento El Teniente y areas adyacentes: Revista Geológica de Chile, v. 27, p. 3–26.

Duarte, P.O., 2000, Caracterización geológica y geotécnica del pórfido dacitico El Teniente: Unpublished Honours thesis, Santiago, Universidad de Chile, 80 p.

Funk, J.A., 2006, Anhydrite-bearing igneous breccias in the El Teniente Cu deposit, Chile: Unpublished Ph.D. thesis, Boulder, University of Colorado, 116 p.

Godoy, E., Yañez, G., and Vera, E., 1999, Inversion of an Oligocene volcano-tectonic basin and uplifting of its superimposed Miocene magmatic arc in the Chilean central Andes: First seismic and gravity evidences: Tectonophysics, v. 306, p. 217–236.

González, R., 2006, Petrografía, geoquímica y microthermometría de los intrusivos félsicos del sector norte del yacimento El Teniente: Unpublished Honours thesis, Chile, Universidad de Concepción, 140 p.

Gustafson, L.B., and Hunt, J.P., 1975, The porphyry copper deposit at El Salvador, Chile: ECONOMIC GEOLOGY, v. 70, p. 857–912.

Gustafson, L.B., and Quiroga, J., 1995, Patterns of mineralization and alteration below the porphyry copper orebody at El Salvador, Chile: ECONOMIC GEOLOGY, v. 90, p. 2–16.

Guzmán, C.G., 1991, Alteración y mineralización de los Pórfidos Dioriticos del sector centrál, yacimiento El Teniente: Unpublished Honours thesis, Santiago, Universidad de Chile, 143 p.

Hitschfeld, M., 2006, Petrografía y geoquímica de los intrusivos leucocráticos del sector sur este del yacimento El Teniente, VI region, Chile: Unpublished Honours thesis, Chile, Universidad de Concepción, 120 p.

Howell, F.H., and Molloy, J.S., 1960, Geology of the Braden orebody, Chile, South America: ECONOMIC GEOLOGY, v. 55, p. 863–905.

Kay, S.M., and Kurtz, A., 1995, Magmatic and tectonic characterization of the El Teniente region: CODELCO-Chile, Internal report, Superintendencia de Geología, El Teniente, 180 p.

Kerrich, R., Goldfarb, R., Groves, D., and Garwin, S., 2000, The geodynamics of world-class gold deposits: Characteristics, space-time distributions, and origins: Reviews in Economic Geology, v. 13, p. 501–551.

Klemm, L.M., Pettke, T., Heinrich, C.A., and Campos, E., 2007, Hydrothermal evolution of the El Teniente deposit, Chile: Porphyry Cu-Mo ore deposition from low-salinity magmatic fluids: ECONOMIC GEOLOGY, v. 102, p. 1021–1045.

Lindgren, W., and Bastin, E.S., 1922, The Geology of the Braden mine, Rancagua, Chile: ECONOMIC GEOLOGY, v. 17, p. 75–99.

Lowell, J.D., and Guilbert, J.M., 1970, Lateral and vertical alteration-mineralization zoning in porphyry copper ore deposits: ECONOMIC GEOLOGY, v. 65, p. 373–408.

Maksaev, V., Munizaga, F., McWilliams, M., Fannning, M., Mathur, R., Ruiz, J., and Zentilli, M., 2004, New chronology for El Teniente, Chilean Andes, from U-Pb, $^{40}Ar/^{39}Ar$, Re-Os, and fission-track dating: Implications for the evolution of a supergiant porphyry Cu-Mo deposit: Society of Economic Geologists Special Publication 11, p. 15–54.

Ossandón, G., 1974, Petrografía y alteración del Pórfido Dacitico, yacimiento El Teniente: Unpublished Honours thesis, Santiago, Universidad de Chile, 112 p.

Quirt, S., 1972, A potassium argon investigation of the Andean mobile belt of North and Central Chile: Unpublished Ph.D. thesis, Queens University, Canada, 240 p.

Riveros, M., 1991, Geología del pórfido latítico del sector sur del yacimiento El Teniente: Unpublished honours thesis, Santiago, Universidad de Chile, 142 p.

Rojas, A., 2003, Porfido Teniente: Dos fases intrusivas caracteristicas geológicas, petrográficas y geoquímicas, yacimiento El Teniente [abs.]: Congreso Geológico Chileno, 10th, Concepción, 2003, Abstracts, p. 9.

Rosenbaum, G., Giles, D., Saxon, M., Betts, P.G., Weinberg, R.F., and Duboz, C., 2005, Subduction of the Nazca Ridge and the Inca Plateau: Insights into the formation of ore deposits in Peru: Earth and Planetary Science Letters, v. 239, p. 18–32.

Seedorff, E., and Einaudi, M.T., 2004, Henderson porphyry molybdenum system, Colarado: I. Sequence and abundance of hydrothermal mineral assemblages, Flow paths of evolving fluids, and evolutionary style: ECONOMIC GEOLOGY, v. 99, p. 3–37.

Seedorff, E., Dilles, J.H., Proffett, J.M., Einaudi, M.T., Zurcher, L., Stavast, W.J.A., Johnson, D.A., and Barton, M.D., 2005, Porphyry deposits: Characteristics and origin of hypogene features: ECONOMIC GEOLOGY 100TH ANNIVERSARY VOLUME, p. 251–298.

Seguel, J., Arévalo, A., and Skewes, M.A., 2006, Complejo de brechas hidrotermales en el flanco este de Mina El Teniente: XI Congreso Geológico Chileno, Antofagasta, Actas, v. 2, p. 351–354.

Sillitoe, R., 1985, Ore-related breccias in volcanoplutonic arcs: ECONOMIC GEOLOGY, v. 80, p. 1467–1514.

——1997, Characteristics and controls of the largest porphyry copper-gold and epithermal gold deposits in the circum-Pacific region: Australian Journal of Earth Sciences, v. 44, p. 373–388.

Skewes, M.A., 1997, Análisis composicionales de las “Andesitas de la Mina” y de plagioclasas en cuerpos intrusivos de El Teniente: Internal report, Superintendencia de Geología, El Teniente, CODELCO-Chile, 22 p.

——1998, Química de intrusivos acidicos del Yacimiento, El Teniente: Internal report, Superintendencia de Geología, El Teniente, CODELCO-Chile, 14 p.

——2006, Intrusivos felsicos del deposito de cobre El Teniente, Chile: Internal report to the Superintendencia Geología de El Teniente, CODELCO-CHILE.

Skewes, A., and Holmgren, C., 1993, Solevantamiento andino, erosión y emplazamiento de brechas mineralizadas en el depósito de cobre porfídico Los Bronces, Chile Centrál (33S): Applicación de geotermometria de inclusiones fluidas: Revista Geólogica de Chile, v. 20, p. 71–83.

Skewes, A.M., and Stern, C.R., 2005, Magmagenesis and mineralization of giant Miocene and Pliocene megabrecccia deposits in the Andes of central Chile [abs.]: Geological Society of America Abstracts with Programs, v. 37, p. 163.

——2007, Geology, mineralization, alteration, and structural evolution of the El Teniente porphyry Cu-Mo deposit—a discussion: ECONOMIC GEOLOGY, v. 102, p. 1165–1170.

Skewes, A.M., Arevalo, A., Floody, R., Zuñiga, P.H., and Stern, C., 2002, The giant El Teniente breccia deposit: Hypogene copper distribution and emplacement: Society of Economic Geologists Special Publication 9, p. 299–332.

——2005, The El Teniente megabreccia deposit: The world's largest copper deposit, *in* Porter, T.M., ed., Super porphyry copper and gold deposits—a global perspective: Adelaide, Australia, Porter Geoscience Consultancy Publishing, v. 1, p. 83–113.

Stern, C.R., 1989, Pliocene to present migration of the volcanic front, Andean Southern Volcanic Zone: Revista Geológica de Chile, v. 16, p. 145–162.

——1991, Role of subduction erosion in the generation of Andean magmas: Geology, v. 19, p. 78–81.

Stern, C., and Skewes, A.M., 1995, Miocene to present magmatic evolution at the northern end of the Andean Southern Volcanic Zone, central Chile: Revista Geológica de Chile, v. 22, p. 261–272.

——2002, Role of mantle-derived mafic magmas in the generation of the giant Miocene and Pliocene copper deposits of central Chile [abs.]: Geological Society of America, Abstracts with Programs, v. 34, p. 88.

Stern, C., Funk, J., Skewes, A. and Arévalo, A., 2007, Magmatic anhydrite in plutonic rocks at the El Teniente Cu-Mo deposit, Chile, and the role of sulfur- and copper-rich magmas in its formation: ECONOMIC GEOLOGY, v. 102, p. 1335–1344.

Valenzuela, R., 2003, Mineralización sulfurada hipógena de cobre en el sector central del yacimiento El Teniente VI region: Unpublished Honours thesis, Chile, Universidad de Concepción, 106 p.

Villalobos, J., 1975, Alteración hídrotermal en las andesitas del yacimiento El Teniente, Chile: Unpublished doctorate thesis, Santiago, Universidad de Chile, 125 p.